Research Square

Preprints are preliminary reports that have not undergone peer review.
They should not be considered conclusive, used to inform clinical practice,
or referenced by the media as validated information.

Impact of Successive Earthquakes on Incremental Structural Damage during the 2025 Sındırgı, Türkiye Earthquake Doublets

Hasan Hüseyin Aydogdu
Istanbul Kültür University
Muhammed Sukru Yavas
Istanbul Technical University
Ugur Demir
ugurdemir@iyte.edu.tr
Izmir Institute of Technology
Alper Ilki
Istanbul Technical University

Research Article

Keywords: Damage, Earthquake doublets, Reinforced concrete, Seismic, Successive earthquakes

Posted Date: November 26th, 2026

DOI: https://doi.org/10.21203/rs.3.rs-11609916/v1

License: This work is licensed under a Creative Commons Attribution 4.0 International License.
Read Full License

Additional Declarations: No competing interests reported.

Impact of Successive Earthquakes on Incremental Structural Damage during the 2025 Sındırgı, Türkiye Earthquake Doublets

Hasan Hüseyin Aydogdu[1], Muhammed Sukru Yavas[2], Ugur Demir[3*], Alper Ilki[4]

[1] *Lecturer, Civil Engineering Department, İstanbul Kültür University, İstanbul, Türkiye*

[2] *Graduate Student, Civil Engineering Department, Istanbul Technical University, İstanbul, Türkiye*

[3*] *Associate Professor, Department of Architecture, İzmir Institute of Technology, İzmir, Türkiye*

[4] *Professor, Civil Engineering Department, Istanbul Technical University, İstanbul, Türkiye*

**Corresponding author e-mail: ugurdemir@iyte.edu.tr*

ABSTRACT

On 10 August 2025, an Mw 6.1 mainshock struck the Sındırgı district of Balıkesir Province, Türkiye, causing widespread structural damage; a second, equally strong earthquake struck the same district on 27 October 2025. This closely spaced sequence makes it possible to examine, in a real-world setting, how successive earthquakes compound damage in structures already weakened by an initial event. To this end, the present study examines two adjacent reinforced concrete (RC) buildings of comparable structural configuration, both classified as heavily damaged after the first earthquake, drawing on detailed field inspection, material testing, and numerical modelling. Comparing the two buildings makes it possible to trace the accumulation of structural damage and assess how pre-existing damage heightens vulnerability to subsequent shaking. Although the two buildings appeared similar at the outset, reconnaissance carried out after the first earthquake revealed specific differences between them that account for their contrasting fates in the second event: one collapsed entirely, while the other remained standing. These findings show how pre-existing damage, compounded by deficiencies in reinforcement detailing, can progressively erode structural capacity under repeated seismic loading.

Keywords: Damage, Earthquake doublets, Reinforced concrete, Seismic, Successive earthquakes

1 INTRODUCTION

Earthquakes often occur in sequences, releasing accumulated tectonic strain through a series of successive ruptures rather than a single event. Although contemporary seismic design codes generally consider a single, rare "design earthquake" scenario, historical seismic doublets and sequences have shown that damage accumulated during one event can trigger collapse in a later one, even when neither shock alone would have been sufficient [1-3]. Such cumulative effects occur because the interval between successive shocks is typically too short for repair or strengthening, leaving structures to enter each new event with reduced stiffness and diminished inelastic capacity [4].

Post-earthquake reconnaissance following recent events in Türkiye and other seismically active regions has consistently underscored the need for systematic assessment of damage distributions and the mechanisms driving seismic losses in existing building stocks. Within Türkiye, damage patterns have been documented in detail following the 1999 Kocaeli and Düzce earthquakes [5-6], the 2011 Van earthquake [7-8], the 2020 Elazığ earthquake [9], the 2020 Aegean Sea earthquake [10-12], and the 2023 Kahramanmaraş earthquake sequence [13-18]. International reconnaissance efforts following major earthquakes elsewhere offer a comparable body of evidence on the seismic performance of existing building stocks. Maeda and Al-Washali [19] examined the structural response of buildings affected by the 1995 Kobe, 2011 Tohoku, and 2016 Kumamoto earthquakes in Japan; in Italy, damage patterns following the 2009 L'Aquila earthquake were reported by Di Ludovico et al. [20] and Kawashima et al. [21]. Kam et al. [22] evaluated the seismic behavior of RC buildings after the 22 February 2011 Christchurch earthquake, while Idris et al. [23] documented post-earthquake damage following the 2016 Pidie Jaya earthquake in Indonesia. These studies demonstrate that a rigorous, field-based understanding of damage mechanisms is essential for meaningful vulnerability characterization and for the timely retrofitting of at-risk structures, a need that becomes especially acute when a region is struck by more than one significant earthquake within a short interval, as occurred in the Sındırgı district of Balıkesir Province in 2025.

In 2025, the Sındırgı district of Balıkesir Province, in western Türkiye, became an unusually well-documented case study of cumulative seismic effects. Situated at the western segment of the active Simav Fault Zone, the region was struck by two significant Mw 6.1 earthquakes within a relatively short time interval. The first mainshock occurred on August 10, 2025, at a shallow focal depth of approximately 7.7 km, resulting in widespread structural damage. Approximately two and a half months later, on October 27, 2025, a second earthquake of comparable magnitude struck the same area, imposing additional cumulative demands on an already damaged building stock. Official damage assessments following the August event reported 20 collapsed buildings and 403 classified as heavily damaged. The ground motion characteristics, aftershock distribution, and damage patterns of the August event were analyzed in detail in the authors' earlier study [24], which found that 95% of the heavily damaged or collapsed buildings had been constructed prior to 1998, a period associated with substandard construction practices, low concrete compressive strengths (6.8-15.2 MPa), and the widespread

use of plain reinforcement bars lacking proper seismic detailing (i.e., insufficient spacing and detailing of lateral reinforcement, or inadequate anchorage/bond).

Following the October earthquake, field reconnaissance teams revisited the areas surveyed after the first event to track the progression of damage in already-affected structures and to document any newly affected buildings. The total number of collapsed buildings rose from 20 to 26, with every additional collapse occurring in a structure that had already been classified as heavily damaged after the August earthquake. Among the observations from this second survey, the most striking was the divergent response of two adjacent RC buildings in the Sındırgı town center, denoted B9 and B10 in the authors' earlier study [24]. Both had been classified as heavily damaged after the first shock and exhibited a similar set of deficiencies: slender columns, a soft-story configuration, insufficient transverse reinforcement, and poor material quality. Yet Building B9 collapsed completely in the October earthquake, while Building B10 remained standing, despite further degradation. Because the two structures entered the second event with nearly identical, independently documented damage states and were subjected to virtually the same ground motion, their contrasting fates constitute an unusually controlled natural experiment on the seismic performance of pre-damaged RC buildings, one rarely available in the post-earthquake reconnaissance literature. This divergence points to geometric regularity, degree of reinforcement corrosion, concrete quality, and the contribution of infill walls as parameters that may govern collapse probability under sequential seismic loading.

This paper presents an integrated study of the Sındırgı earthquake sequence, aimed at clarifying how damage accumulates incrementally and structural integrity is progressively lost over successive seismic events. Existing reconnaissance studies have documented damage distributions after individual earthquakes in considerable detail [5-23], yet none has systematically quantified how a documented pre-event damage state governs structural response, collapse probability, and capacity degradation when the same structure is subsequently subjected to a second, comparably strong earthquake. To the authors' knowledge, no previous field study has paired sequential, quantified damage statistics with nonlinear numerical modeling of the same pre-damaged RC buildings before and after a second major event, a combination that the Sındırgı sequence, with its two closely spaced Mw 6.1 earthquakes and the pre-existing damage documentation from [24], makes possible for the first time. The present study addresses this gap by integrating three complementary components: a seismological characterization of the earthquake sequence, updated comparative damage statistics from the August and October surveys, and a detailed structural assessment of Buildings B9 and B10. Ground motion characteristics, including the temporal and spatial distribution of aftershocks and comparisons of spectral accelerations, are examined first, followed by an evaluation of how the citywide damage distribution evolved between the two events. The structural response of Buildings B9 and B10 is then investigated in detail, drawing on geometric and material characterization together with nonlinear finite element modeling. Incremental damage accumulation is quantified through nonlinear time-history analysis using fiber-based section models that explicitly incorporate the buildings' documented pre-event damage states, allowing the effect of that damage on subsequent seismic performance to be

isolated rather than inferred. In doing so, this study provides field-calibrated, quantitative evidence, rather than purely analytical or laboratory-based evidence, of collapse triggered by a seismic doublet, and identifies the specific structural parameters that differentiated a total collapse from a surviving, further-degraded building under nominally identical repeated ground motion. The findings underscore the governing role of cumulative damage in structural performance and point to the need for rapid, targeted post-earthquake assessment and retrofitting protocols for RC building stocks exposed to sequential seismic loading.

2 2025 SINDIRGI EARTHQUAKE SEQUENCE

The 2025 Sındırgı earthquake sequence began with a mainshock of magnitude Mw 6.1 on August 10, 2025, at 19:53 local time (39.2403° N, 28.0587° E). This event was followed by several significant aftershocks over the subsequent three months. The largest aftershocks occurred on August 24, 2025 (Mw 4.8), September 7, 2025 (Mw 4.9), and September 21, 2025 (Mw 4.9). In addition, a second major earthquake with a magnitude of Mw 6.1 occurred on October 27, 2025. These two Mw 6.1 events are identified as the main earthquakes of the sequence. Performed analyses indicate that both main earthquakes had shallow focal depths of approximately 7-8 km, consistent with the characteristic crustal mechanism of the region. Accelerometer records obtained from station 1015, located in the town of Sındırgı, captured strong ground motions with peak ground accelerations (PGA) ranging from 0.046g to 0.38g across the two main earthquakes and three major aftershocks, resulting in a total of five consecutive seismic events (Fig. 1). Location of the epicenters is shown on the PGA map through Fig. 2. The response spectra derived from the accelerometer recordings were compared with the DD-2 level design spectrum (Fig. 3). This corresponds to a strong ground motion with a return period of 475 years (10% probability of exceedance in 50 years) and is defined as the elastic design spectrum in the 2018 Turkish Building Earthquake Code [25]. The results indicate that the August 10 earthquake exhibited dominant spectral accelerations in the period range of 0.8-1.2 s, whereas the October 27 earthquake showed higher amplification at shorter periods, primarily between 0.4 and 0.8 s. Although both events produced comparable PGA values, the second earthquake imposed significantly higher demands at shorter periods (Fig. 3), which is particularly critical for low and medium-rise RC and masonry buildings, typical of the Sındırgı urban area.

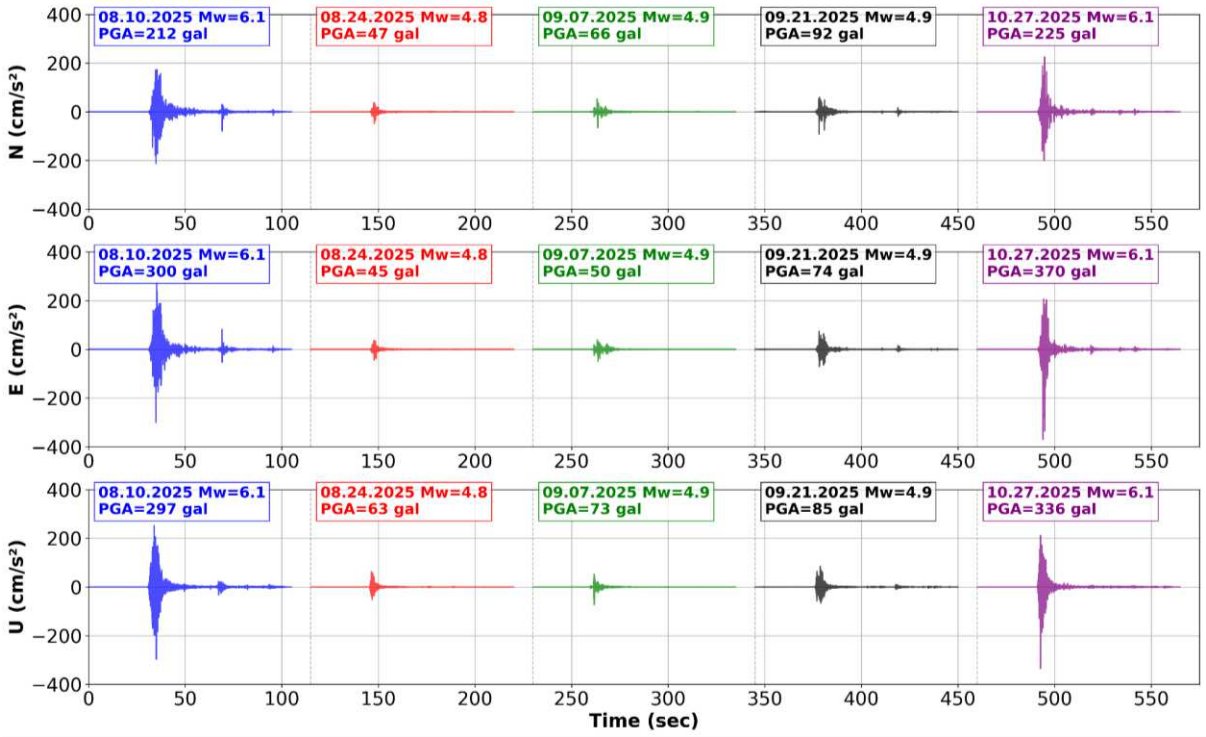

Figure 1: Acceleration time histories for 5 major events

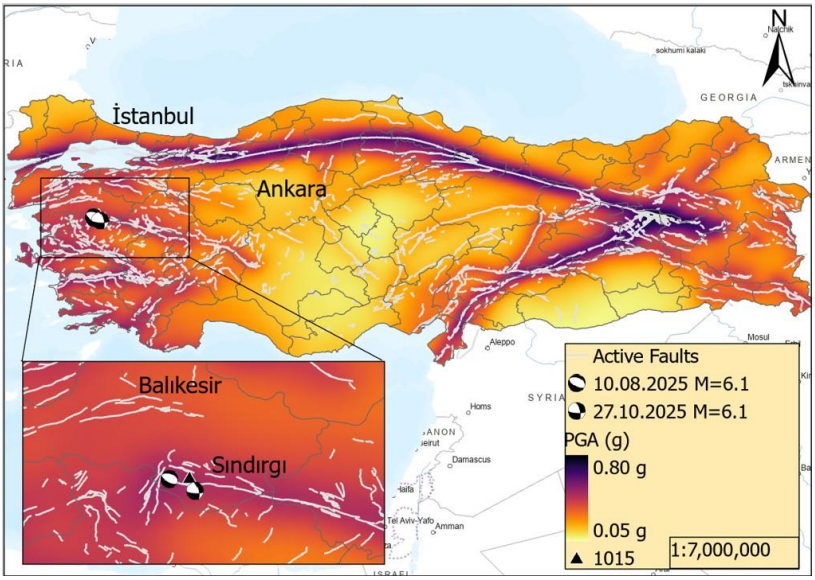

Figure 2: Location of the epicenters on the PGA map of design-level earthquake defined by the Turkish Seismic Hazard Map [26]

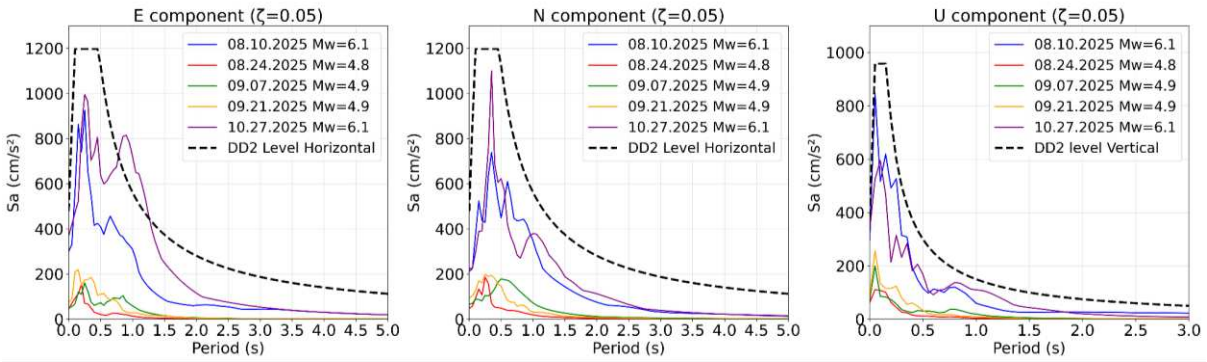

Figure 3: Response spectrum for 5 major events

Aftershock analyses and distribution of earthquakes by magnitude are shown in Figs. 4 and 5, respectively. Figure 4 demonstrates a gradual decay in event frequency, yet with several moderate shocks persisting beyond two months. Spatial distribution maps (Figs. 6 and 7) show that most aftershocks including the second main shock were concentrated along the east-west trending fault system extending between Alakır and Sındırgı, overlapping with the rupture zone of the first mainshock. The persistence of aftershocks and the recurrence of strong shaking over a short period likely contributed to cumulative structural degradation, particularly in already damaged buildings. Moreover, Fig. 6 presents the spatial distributions of PGA, PGV, and spectral accelerations at periods of 0.3 s and 1.0 s for the first and second Mw = 6.1 earthquakes. The shakemaps indicate that the first earthquake generated stronger ground-motion demands in the western regions of the Sındırgı district, whereas the second earthquake produced higher demands around the east of the district. In the Sındırgı city center, the intensity measures associated with the second Mw = 6.1 earthquake were slightly higher than those of the first earthquake. To further examine the amplitudes of the two mainshocks relatively, Figs. 7a and 7b demonstrate the ratios of the spectral acceleration demands of the second earthquake to those of the first earthquake at periods of 0.3 s and 1.0 s, respectively. Ratio values greater than 1.0 indicate locations where the second earthquake resulted in higher spectral acceleration demands than the first earthquake. The ratio maps confirm that the first earthquake was more demanding in the western part of the district, whereas the second earthquake dominated in the eastern part. In the Sındırgı city center, the spectral demands generated by the two earthquakes were comparable, with both events producing sufficiently high shaking intensities to cause structural damage. Nevertheless, the second earthquake caused slightly higher spectral acceleration demands, suggesting a marginally more severe seismic input for the buildings located in the city center.

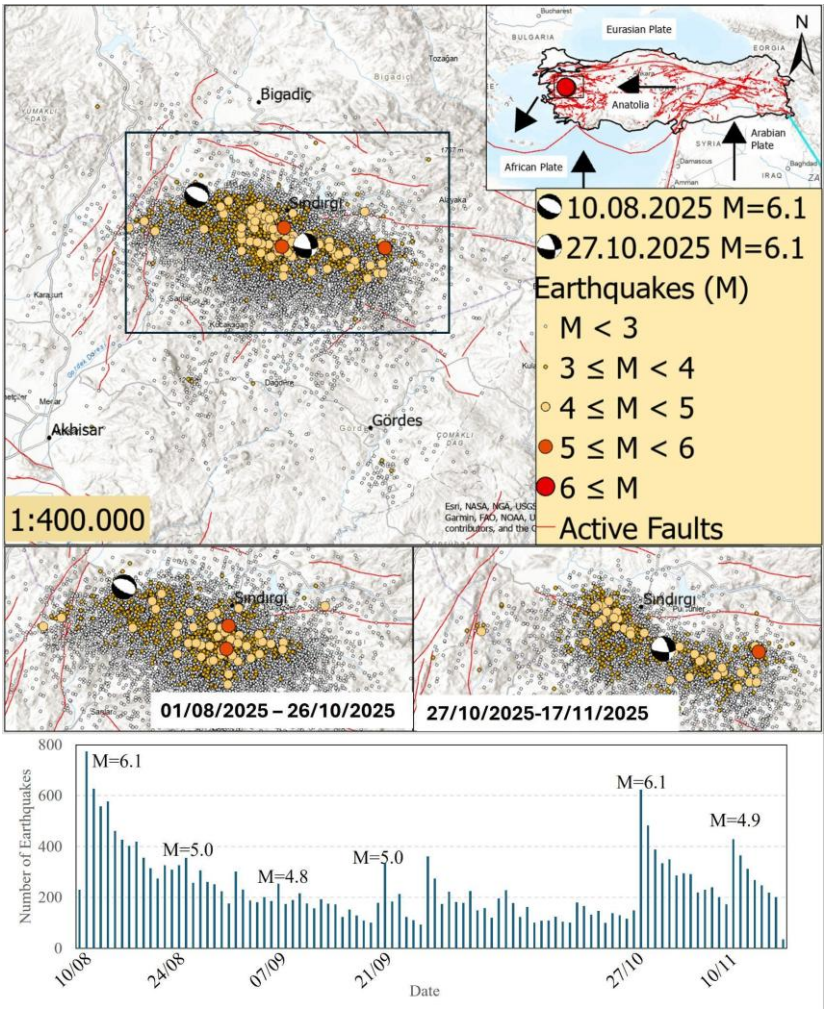

Figure 4: Spatial distribution of the mainshock and the aftershocks

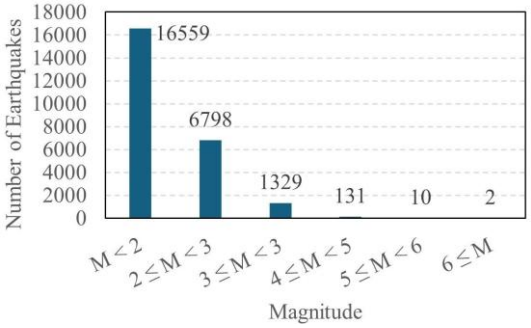

Figure 5: The distribution of earthquakes by magnitude

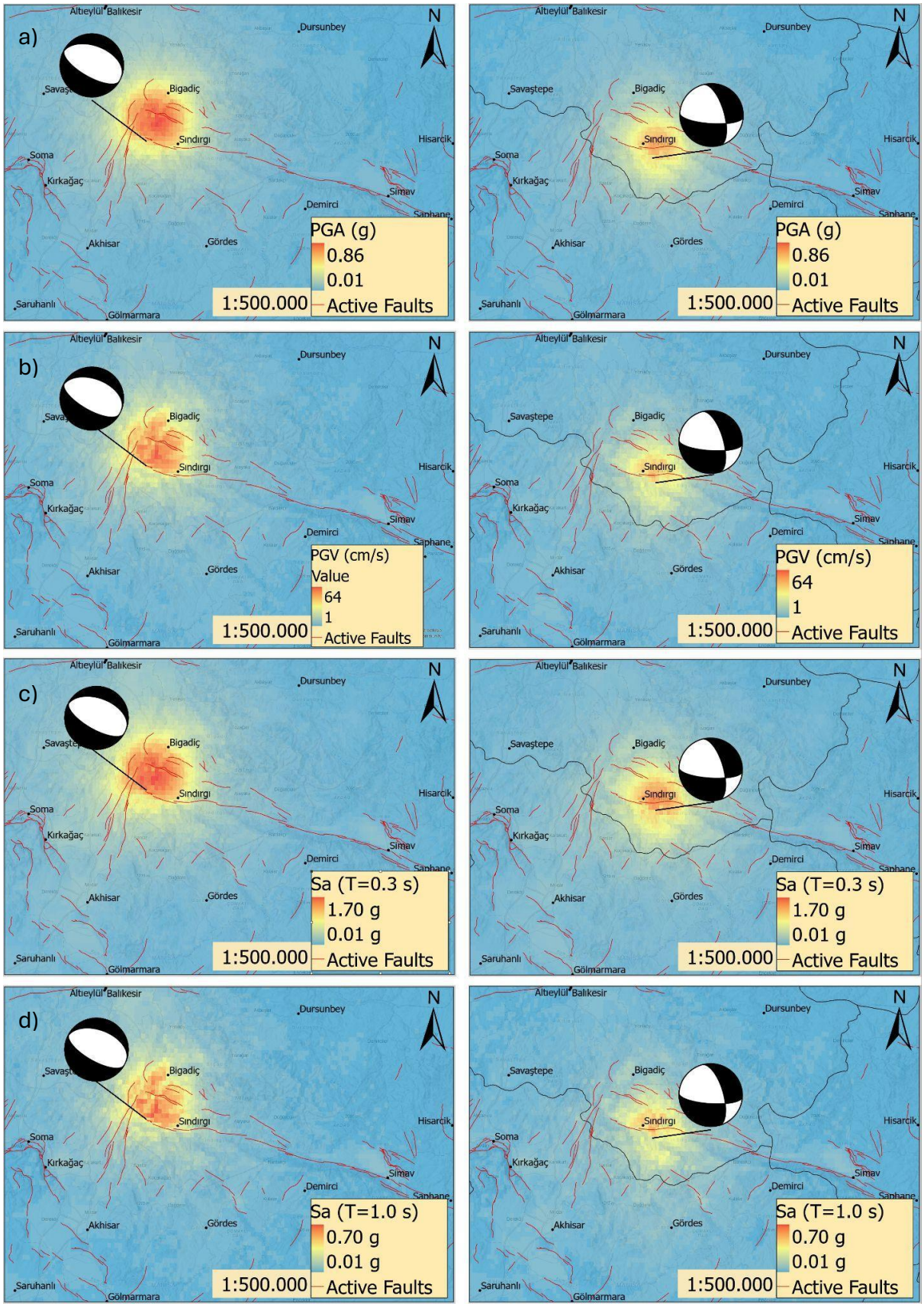

Figure 6: Shakemap provided by USGS (2025) [27]: (a) PGA, (b) PGV, (c) spectral acceleration at 0.3 s period, (d) spectral acceleration at 1.0 s period. Left column: first earthquake; right column: second earthquake.

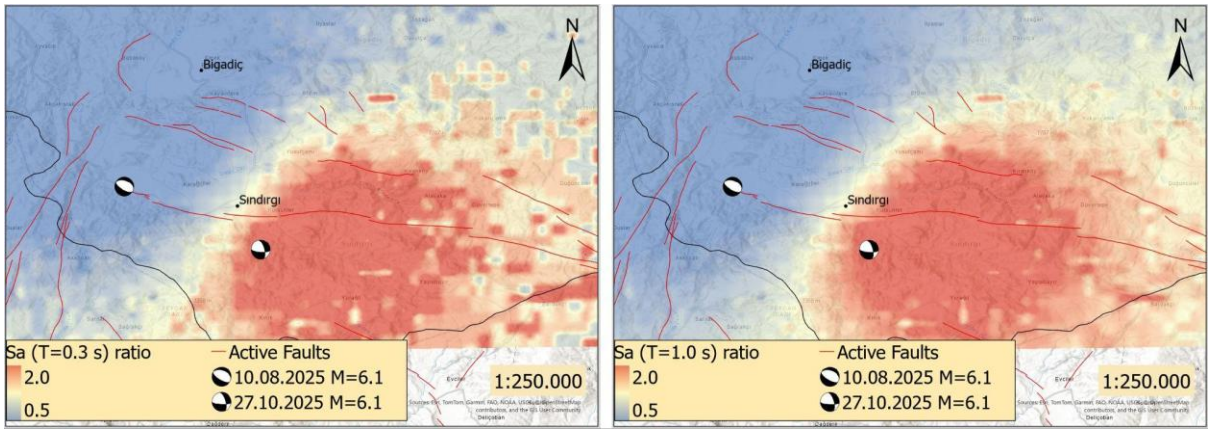

Figure 7: The estimated median spectral acceleration value ratio of the second earthquake to the first earthquake. The estimated ground motion parameters are provided by USGS Shakemaps [27].

3 POST-EARTHQUAKE STRUCTURAL DAMAGE ASSESSMENT

3.1 Methodology

Post-earthquake damage assessments were launched by the Ministry of Environment Urbanization and Climate Change (MEUCC) immediately after both seismic events. The inspections were conducted in accordance with the post-earthquake damage assessment guidelines issued by Disaster and Emergency Management Presidency (AFAD) [28] in Türkiye, adopting a decision logic and damage classification scheme that are largely consistent with the methodology introduced by Ilki et al. [29]. In this methodology, buildings are categorized into six global damage states, namely no damage (ND), slight damage (SD), moderate damage (MD), heavy damage (HD), urgent demolition (UD), and collapse (C), based on observed earthquake-induced structural damages. Field reconnaissance and damage evaluations were carried out by trained expert teams affiliated with MEUCC, typically consisting of civil engineers and/or architects. Prior to deployment, these teams underwent both technical training and orientation sessions to ensure consistency in assessment procedures. The evaluation protocol initially involves a comprehensive exterior survey, during which global structural response indicators such as permanent lateral drifts, differential settlement, and rigid-body rotations are examined. Buildings that do not exhibit signs of collapse, partial collapse, or severe global instability during the exterior inspection phase are subsequently subjected to interior investigations. Interior inspections focus on identifying and documenting damage to structural components located at the most severely affected story.

For RC buildings, observed damage to vertical load-bearing elements (columns, shear walls, joints) as well as horizontal members (beams) is classified into five discrete damage levels. These include: Type O, representing undamaged members; Type A, indicating the presence of hairline or minor cracks (≤0.5 mm); Type B, corresponding to moderate cracking (0.5-3 mm) and/or localized crushing/spalling of the concrete cover; Type C, denoting severe cracking (>3 mm) and/or slight buckling of the longitudinal reinforcement; and Type D, associated with core concrete crushing, reinforcement buckling or fracture, and/or pronounced residual deformations (Table 1).

Table 1. Damage classification table for RC structural members [28]

Damage class	Crack width	Damage	Damage factor
O	-	-	0.0
A	w ≤0.5 mm	-	0.2
B	0.5< w ≤3.0 mm	Crushing of concrete cover, spalling of concrete cover	0.4
C	w > 3.0 mm	Slight buckling of reinforcement (Buckling (δ) ≤ Stirrup spacing (s)/20 and 1.5 cm)	0.7
D	-	Rupture of reinforcement Crushing of core concrete Residual shortening Residual shear deformations Buckling of reinforcement (Buckling (δ) > Transverse bar spacing (s)/20 or 1.5 cm)	1.0

Within the assessment procedure, RC buildings are first classified into three categories based on plan area and number of stories: Category 1 comprises buildings with a base area smaller than 600 m² and no more than 10 stories; Category 2 comprises buildings with a base area exceeding 600 m² or with more than 10 but no more than 15 stories; and Category 3 comprises all buildings with more than 15 stories, or those incorporating special structural elements such as base isolators or dampers, as well as industrial structures, all of which are directed to a mandatory detailed assessment. For Categories 1 and 2, an exterior (rapid) inspection is first performed to check for partial or total collapse and for excessive settlement, rotation, or permanent lateral drift; in the absence of such conditions, the building proceeds to an interior (detailed) inspection. In this regard, the Category 1 Assessment procedure classifies buildings according to the extent of damage observed in structural members, without requiring a quantitative damage index. If none of the vertical or horizontal structural elements exhibit critical (Type C or D) damage, the building is rated as undamaged or slightly damaged, depending on whether non-structural elements are damaged. Otherwise, if at least one vertical or horizontal structural member exhibits Type C or D damage on the inspected floor, the assessment proceeds to Category 2. In the Category 2 procedure, each vertical structural member is first classified into one of five damage classes (O, A, B, C, or D) based on observed crack widths and failure modes, as summarized in Table 1. Each damage class is assigned a damage factor, ranging from 0 for undamaged members (Class O) to 1 for members exhibiting severe damage such as reinforcement rupture or core concrete crushing (Class D). If the inspected story contains vertical or horizontal structural members classified as Type C or D, a Weighted Damage Percentage for Vertical Members (WDPVM) is computed for the most heavily damaged story, as shown in Eq. (1). In this equation, O, A, B, C, and D denote the total cross-sectional areas of vertical structural members (columns and structural walls) classified in the corresponding damage class (O, A, B, C, or D, respectively) at the most heavily damaged story under consideration, and the coefficients are the damage factors listed in Table 2,

reflecting the relative severity of each damage class. A WDPVM value exceeding 60% indicates that the building has lost a critical portion of its lateral load-carrying capacity and results in an immediate classification as requiring emergency demolition.

$$WDPVM = 100 \times \frac{(A\times 0.20+B\times 0.40+C\times 0.70+D\times 1.00)}{(O+A+B+C+D)} \quad (1)$$

Table 2. Detailed damage evaluation procedure decision algorithm for RC buildings [28]

Determination of building damage category		**Columns / Shear Walls / Joints**			
		WDPVM < 10 and C+D = 0	**10 ≤ WDPVM < 20 or WDPVM < 10 and C+D ≥ 1**	**20 ≤ WDPVM < 40**	**WDPVM ≥ 40**
Beams	**C ≤ FA/50 and D = 0**	Slightly Damaged	Moderately Damaged	Moderately Damaged	Heavily Damaged
	C+D < FA/50 and D ≥1	Moderately Damaged	Moderately Damaged	Heavily Damaged	Heavily Damaged
	FA/50≤ C+D <FA/20	Moderately Damaged	Moderately Damaged	Heavily Damaged	Heavily Damaged
	C+D ≥ FA/20	Heavily Damaged	Heavily Damaged	Heavily Damaged	Heavily Damaged

FA: Footprint area of the building.

For masonry buildings, the classification and inspection scheme follows a similar logic. Buildings are grouped by the number of free stories into two categories: Category 1 (five or fewer stories) and Category 3 (more than five stories) proceed through the standard exterior-then-interior inspection sequence, while registered masonry structures forming part of the cultural heritage are directed to detailed inspection regardless of number of stories. There is no Category 2 classification for the masonry unlike RC buildings. During interior inspection, the presence of differential foundation settlement or rotation beyond acceptable limits results in an immediate heavy-damage classification; otherwise, if all structural elements on the inspected floor are undamaged (O type), the building is rated as undamaged or slightly damaged depending on whether non-structural damage is present. Each masonry wall element is assigned a damage class based on crack width and material condition (Table 3). If the inspected floor contains at least one wall with D-type damage, at least two walls with C-type damage, or a staircase with D-type damage, the building is classified as heavily damaged; otherwise, it is classified as slightly damaged.

Table 3. Damage classification table for masonry structural members [28]

Damage class	Crack width	Damage
O	-	-
A	w ≤1.0 mm	Minor cracking
B	1.0< w ≤5.0 mm	Moderate cracking and/or mortar disintegration or loss

C	5.0< w ≤10.0 mm	Severe cracking and/or crushing of masonry units
D	w > 10.0 mm	Pronounced wall deformations, significant loss of structural integrity

3.2 Structural Damage Assessment After the First Earthquake (10 August 2025)

Following the above-mentioned damage assessment methodology, the analysis of the structural damage stemming from the first earthquake indicated that the first event caused considerable damage to both RC and masonry buildings, particularly in rural settlements with a predominance of non-engineered stone and brick construction [24]. The post-earthquake damage assessment of over 20,674 structures after the first earthquake revealed that 20 buildings collapsed, 16 were to be urgently demolished, and 413 were heavily damaged (Fig. 8). The seismic performance in Sındırgı varied significantly between the city center and rural settlements due to differences in structural typology and construction quality. Masonry buildings dominated the building stock district-wide, but their prevalence was especially high in rural areas. Although the damaged buildings mostly consisted of slightly damaged ones, the collapse pattern exposed clear vulnerabilities of non-engineered masonry systems. Of the 20 collapsed buildings, 19 were unreinforced masonry houses located in rural areas, while only one was an RC building in the city center. The detailed damage statistics emphasized that seismic risk in Sındırgı is strongly linked to construction practices and building age. Heavily damaged or collapsed buildings were predominantly one or two-story masonry residences with poor wall connections and weak roof anchorage, reflecting the characteristics of traditional village dwellings. Approximately 95% of the buildings beyond heavy and further (heavy, to be urgently demolished and collapsed, hereafter heavy^{+}) damage was constructed before 1998, when seismic code enforcement and engineering supervision were minimal, as the currently existing inspection/control mechanism was not effectively enforced. In contrast, post-2000 buildings, designed under newer codes with improved materials, showed significantly better performance, with no collapses recorded and only two structures sustaining heavy damage: a six-story RC building constructed in 2005 and a non-engineered masonry house in a rural settlement. It is noteworthy that no buildings were classified as moderately damaged, for both administrative and structural reasons. Administratively, past earthquake experience showed that moderately damaged buildings were typically directed toward retrofitting; however, in rural areas, retrofitting was often deemed impractical given site accessibility and limited engineering services, so damaged buildings were classified either as slightly or heavily damaged rather than moderately damaged. Structurally, both masonry and RC buildings exhibited brittle behavior, sustaining either light cracking within the elastic range (slight damage) or severe cracking, crushing, and deformation once their strength capacity was exceeded (heavy damage), with no intermediate ductile response. These combined administrative and structural factors explain the absence of a "moderate damage" category in the dataset. More details of the damage assessment conducted after the first earthquake have been reported in the earlier paper of the authors [24].

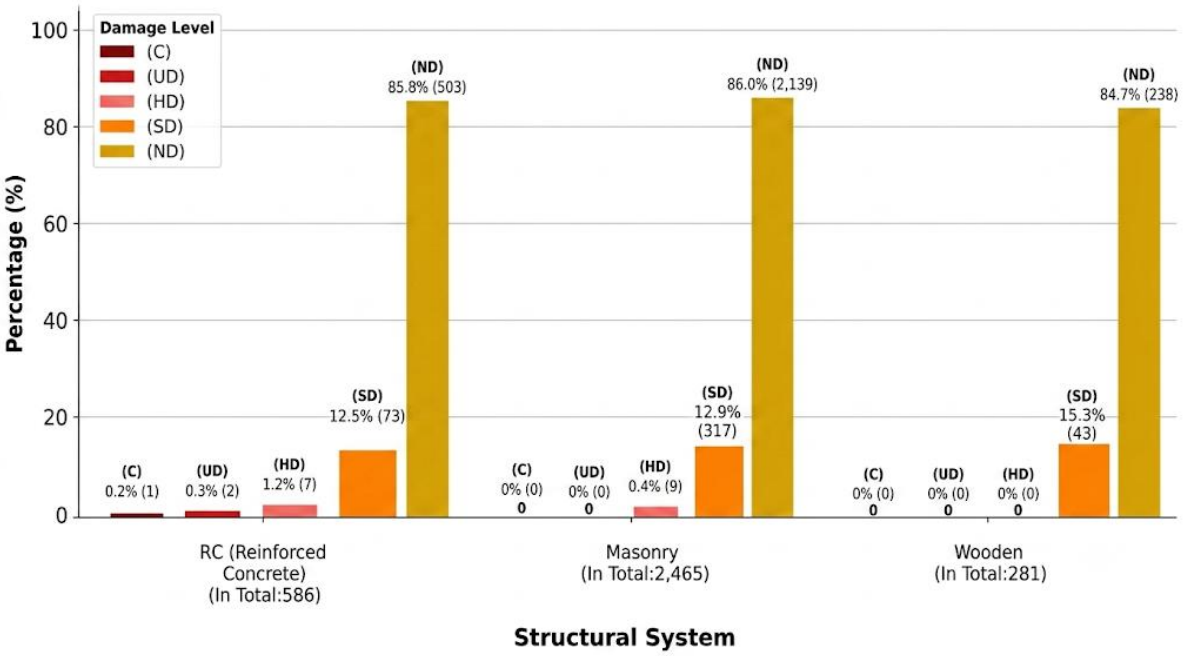

a) City Center

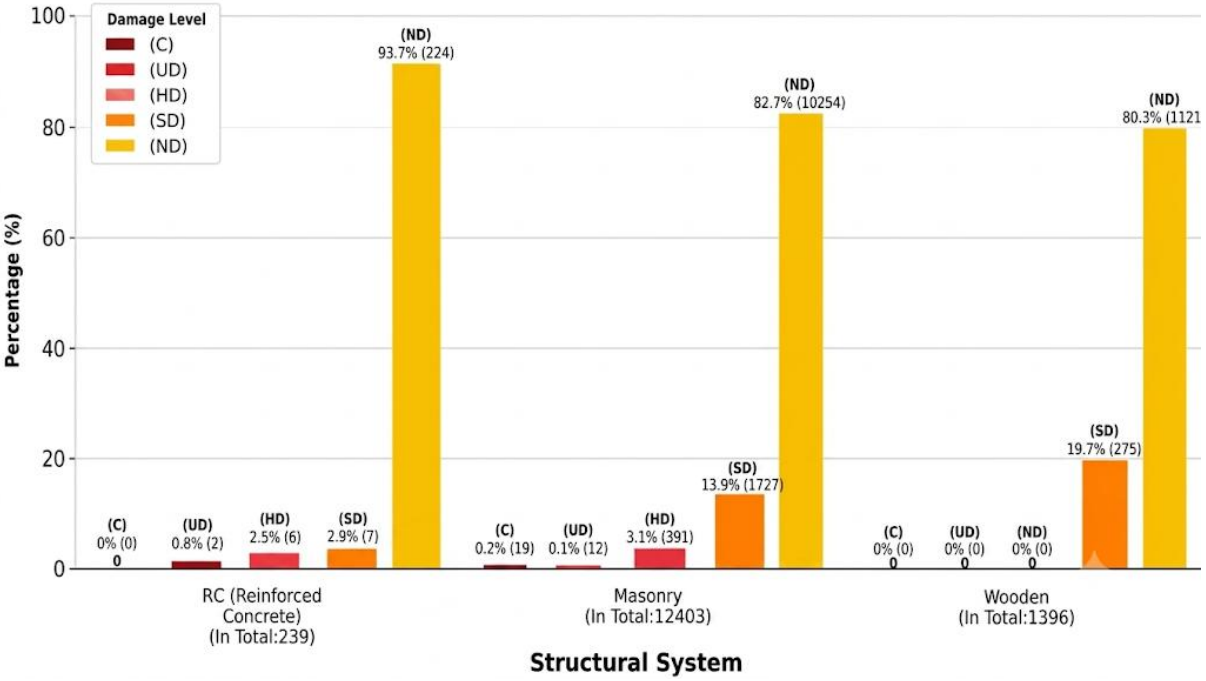

b) Rural

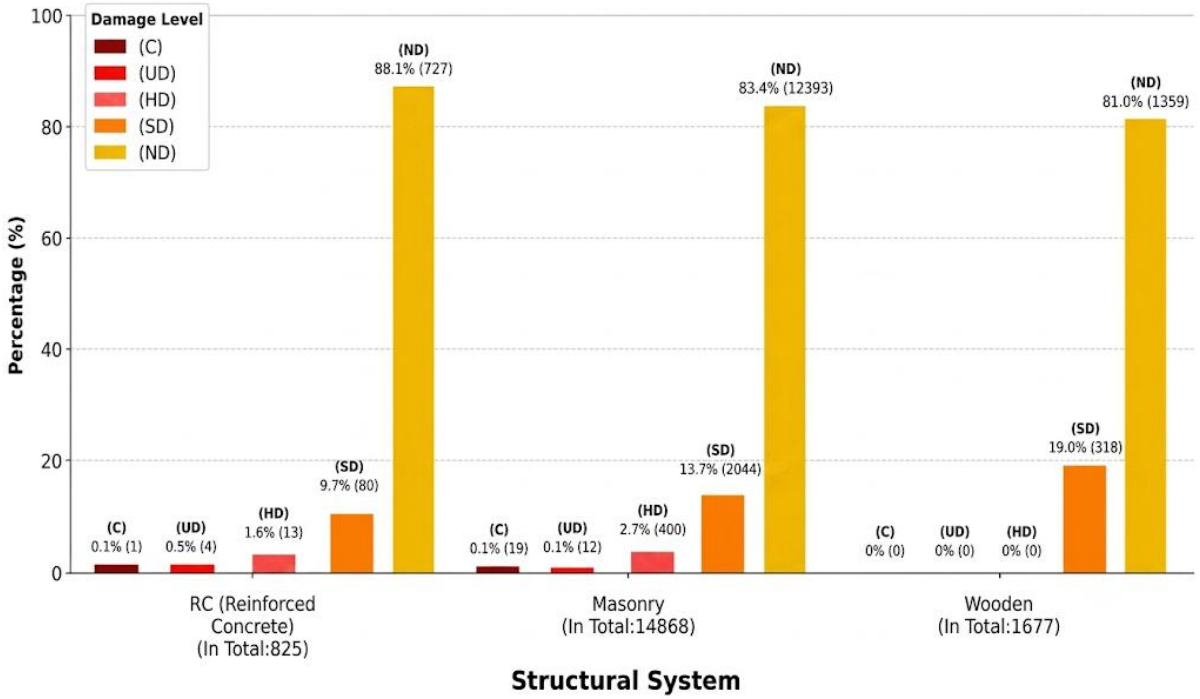

c) All

Figure 8: Damage level distribution for the 10 August 2025 Sındırgı earthquake (The first damaging earthquake sequence)

3.3 Structural Damage Assessment After the Second Earthquake (27 October 2025)

Following the Mw 6.1 Sındırgı earthquake of 27 October 2025 (the second damaging earthquake of the sequence), another comprehensive post-earthquake damage assessment was conducted for 21,858 buildings by the technical teams of MEUCC, encompassing both the urban center (4,300 buildings) and surrounding rural settlements (17,558 buildings) (Fig. 9). This large-scale dataset enabled a detailed evaluation of damage distribution across structural typologies, while also allowing a direct comparison with the damage state observed after the preceding 10 August 2025 Mw 6.1 earthquake (the first damaging earthquake of the sequence). Such sequential assessment provided a valuable opportunity to examine damage accumulation under repeated seismic loading, an issue increasingly emphasized in recent earthquake engineering literature [30-31]. Once the damage data is assessed, a pronounced contrast between urban and rural building stocks was observed like the previous earthquake. In the city center, engineered structures are relatively more prevalent. RC buildings constitute approximately 40% of the stock, while masonry buildings account for about 52%. In rural areas, however, masonry construction overwhelmingly dominates, representing nearly three-quarters (73.8%) of all buildings, whereas RC structures comprise only 15.7%. This urban-rural disparity strongly influenced the observed damage patterns and is consistent with post-earthquake reconnaissance findings from Türkiye and other regions characterized by extensive non-engineered construction [32-33]. Overall damage distributions (Fig. 10) indicate that most buildings remained in the ND or SD categories; nevertheless, disaggregation by structural typology reveals markedly different performance trends. Moreover, RC buildings were seen exhibiting comparatively stable behavior across both earthquakes. In the urban center, nearly

80% of evaluated RC buildings remained classified as ND after the October event, with only a very small fraction was in MD or HD states. However, this outcome should be interpreted with caution, as it is largely attributable to the moderate magnitude of the seismic events rather than to the inherent seismic adequacy of the building stock. Importantly, a similar ND ratio (approximately 84%) was also observed for evaluated RC buildings in rural areas, despite known deficiencies in construction supervision. In contrast, masonry buildings, particularly the ones located in rural settlements, demonstrated significantly higher vulnerability to sequential seismic loading. While roughly two-thirds of evaluated urban masonry buildings remained ND, the proportion of heavily damaged masonry structures increased noticeably during the second earthquake, with damage transitions from ND or SD to heavy damage observed in a non-negligible subset. This transition is more clearly underlined in the next chapter of the study, and the trend is consistent with well-established vulnerability models for unreinforced masonry, which emphasize brittle failure modes, limited deformation capacity, and a pronounced sensitivity to prior cracking and loss of integrity [34-35]. On the other hand, hybrid structural systems, typically combining RC frames with masonry walls, displayed intermediate and more heterogeneous behavior. In the urban center, approximately 70% of hybrid buildings remained ND, while a noticeable portion transitioned to SD or HD. This response can be interpreted as reflecting the complex interaction between relatively ductile RC components and brittle masonry elements, where incompatibilities in stiffness and deformation capacity can lead to localized damage concentrations. Such mechanisms have been widely reported in studies of mixed structural systems subjected to seismic loading and are particularly relevant in regions where incremental construction practices prevail [36-37].

From a damage assessment and risk mitigation perspective, these results emphasize several critical points. First, buildings must be re-evaluated after subsequent earthquakes, even if initial damage appears minor, as reliance on single-event damage classification can create a false sense of safety. Second, prioritization strategies for strengthening or demolition should explicitly incorporate damage history, particularly for masonry structures in rural areas. Screening methods and loss models that neglect cumulative damage effects are likely to underestimate risk in earthquake sequences. Finally, while seismic code advancements have demonstrably improved the performance of newer RC buildings, the persistence of non-engineered masonry construction, especially the ones in rural settlements, continues to dominate regional seismic risk, highlighting the need for targeted policy and technical interventions.

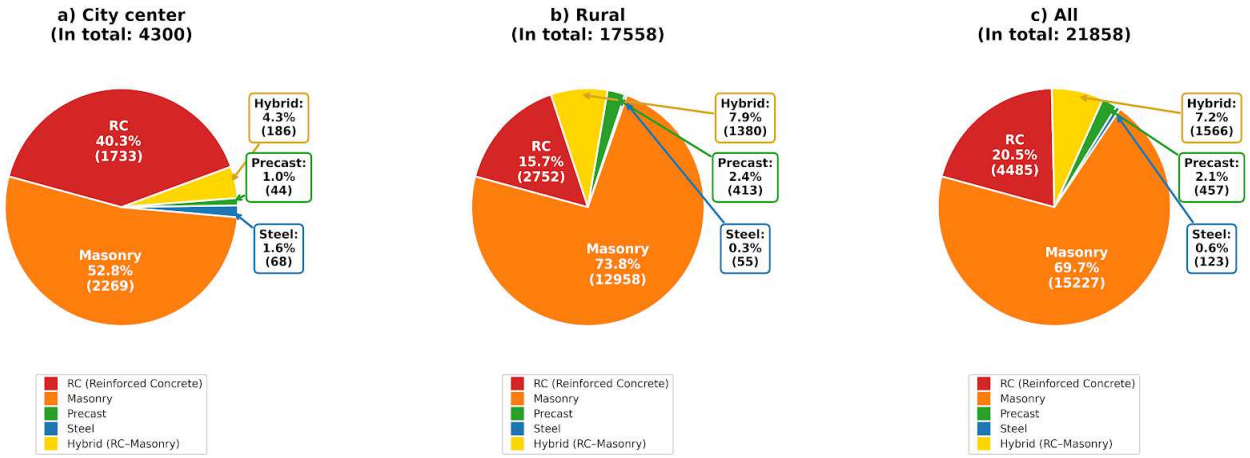

Figure 9: Structural systems of the buildings investigatedafter the 27 October 2025 Sındırgı earthquake (The second damaging earthquake of the sequence)

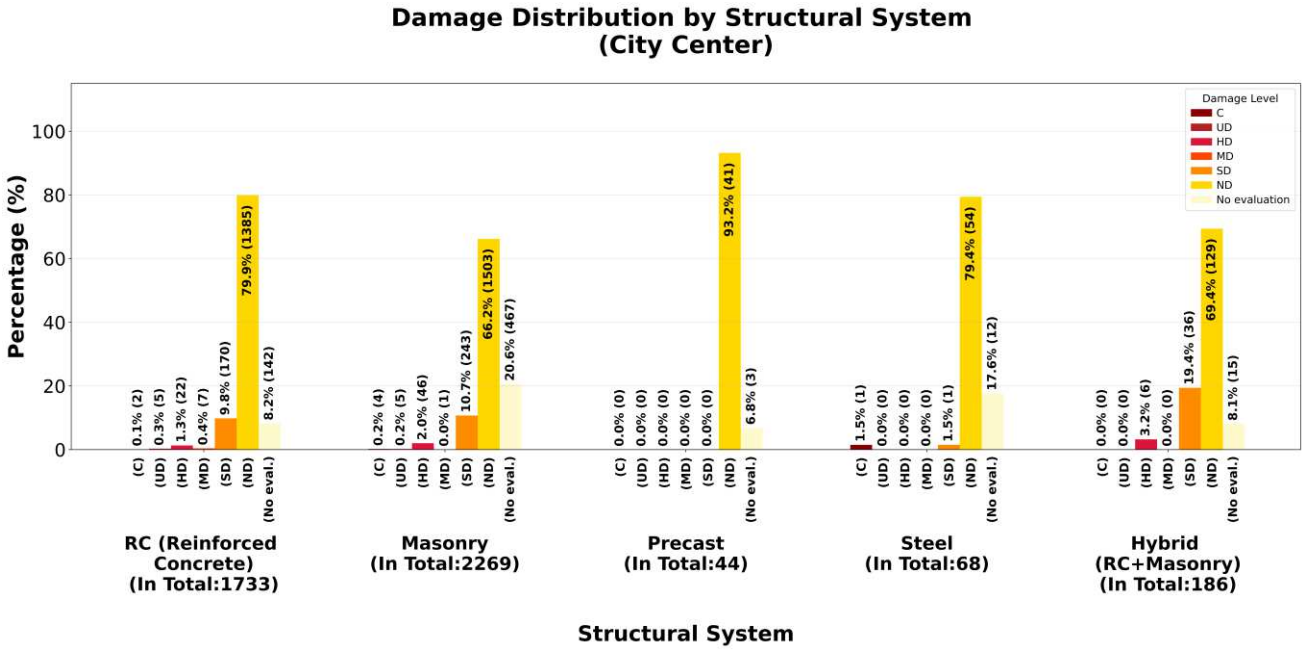

a) City Center

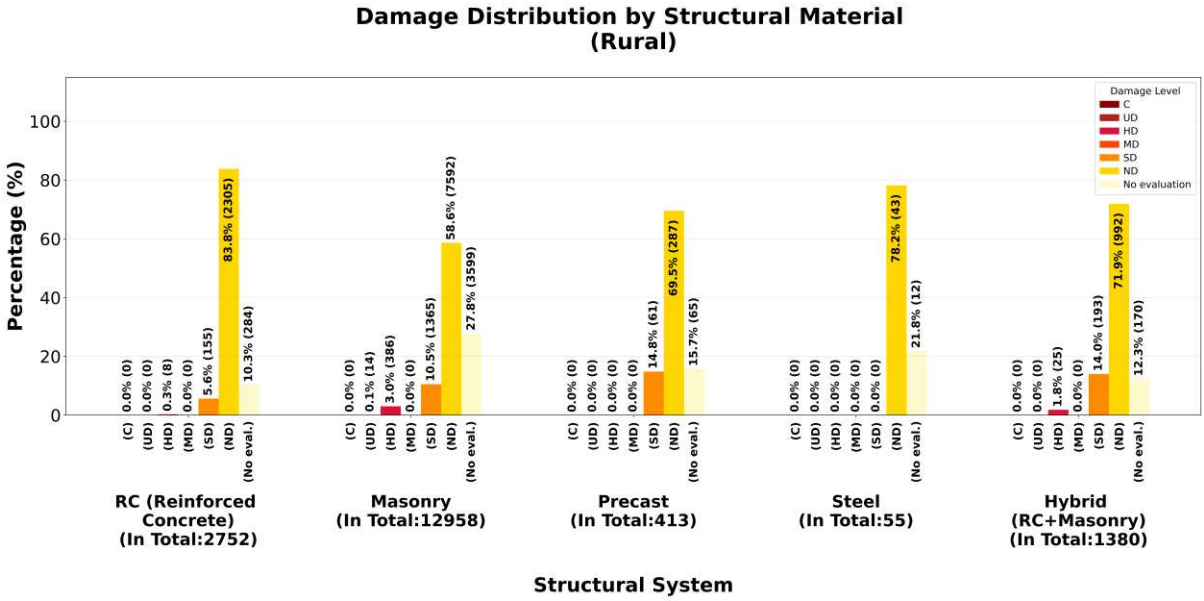

b) Rural

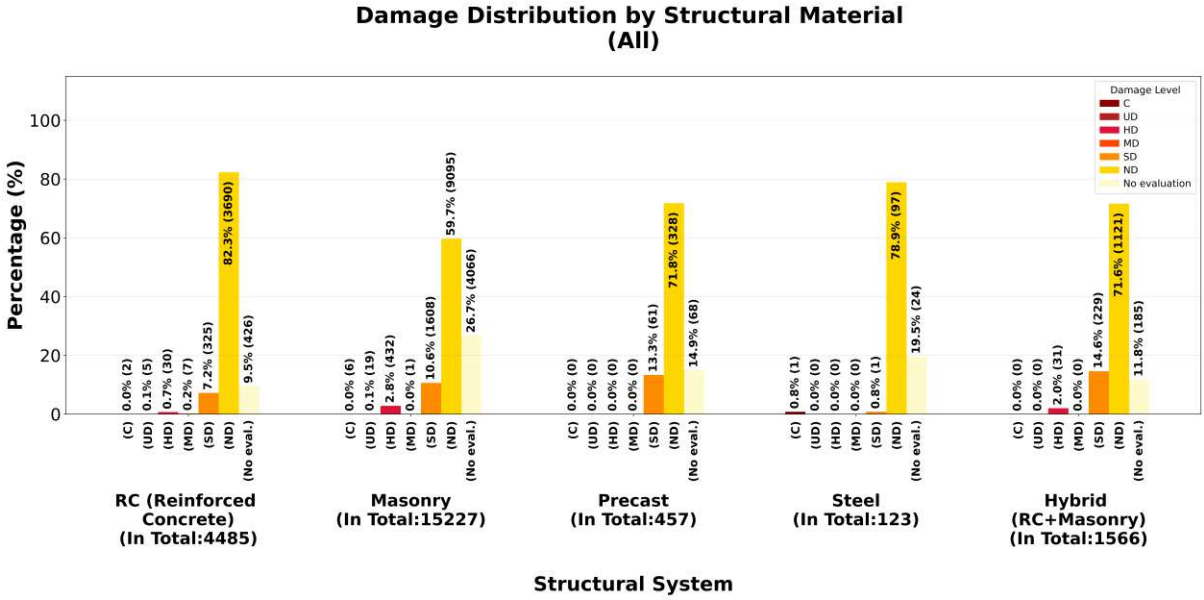

c) All

Figure10: Damage level distribution for the buildings by structural material for the 27 October 2025 Sındırgı earthquake (The second damaging earthquake of the sequence)

Detailed damage statistics following the second earthquake are presented in Tables (4-6), demonstrating that seismic performance is strongly influenced by construction year, number of stories and occupancy type. Table 4 indicates that construction period is the most decisive parameter. In the city center, no post-2000 buildings exhibited heavy or further (heavy^{+}) damage, whereas in rural areas only two buildings constructed after 2000 experienced heavy^{+} damage. Approximately 90% of post-2000 RC buildings remained undamaged (ND), with ND counts approaching 3,000 across all structural systems, while the pre-2000 building stock accounted for the vast majority of severe damage cases. Similarly, only 20 post-2000 masonry

buildings in rural areas were classified as heavy^{+}, and none were recorded in the city center. Notably, nearly 60% of masonry buildings constructed before 2000 were still categorized as ND, indicating partial but insufficient performance within older stock. Precast and steel structures, although limited in number, demonstrated satisfactory performance, with nearly all cases classified as ND. Hybrid systems, where the ground floor was mostly built of stone and the upper floors of brick, also showed high ND ratios in newer construction; however, pre-2000 hybrid buildings exhibited noticeable weaknesses, confirming that outdated construction practices significantly reduce seismic performance. Table 5 presents the damage distribution according to the number of stories. Buildings with 0-2 stories constitute approximately 93% of the evaluated stock, representing the dominant typology in the region. Within this group, only 8 RC buildings (1 in the city center and 7 in rural areas) and 449 masonry buildings (47 in the city center and 402 in rural areas) experienced heavy^{+} damage. These results suggest that low-rise configuration alone does not guarantee adequate seismic performance, particularly for non-engineered masonry structures in rural settings. Table 6 illustrates the relationship between occupancy type and damage class. Residential buildings dominate the dataset. Among 3,825 RC residential buildings, only 16 were classified as heavy^{+}, whereas 376 out of 13,446 masonry residential buildings exhibited heavy^{+} damage. In contrast, no heavy^{+} damage was recorded in public buildings (e.g., schools, government buildings, mosques), indicating comparatively higher performance, likely attributable to stricter supervision and maintenance practices. Tables (4-6) together support three overarching conclusions. First, construction year is the strongest predictor of seismic performance, with post-2000 buildings consistently demonstrating ND ratios of approximately 90%. Second, structural system plays a decisive role: RC buildings outperform masonry structures in terms of exposure to heavy^{+} damage, particularly given the limited engineering input typically associated with masonry construction. Third, occupancy type influences vulnerability patterns, with public buildings generally exhibiting superior performance, residential buildings showing mixed outcomes, and rural auxiliary or abandoned structures representing the most fragile category. Overall, the findings clearly indicate that compliance with modern seismic codes, the prevalence of engineered RC systems, and enhanced standards applied to public buildings contribute significantly to improved seismic performance, whereas older construction, rural building practices, and auxiliary structures require prioritized retrofitting and more rigorous evaluation to effectively reduce seismic risk.

Table 4: Damage level distribution by construction year for the 27 October 2025 Sındırgı earthquake (The second damaging earthquake of the sequence)

Structural System	Damage Level	<1975	1975-2000	2000-2007	2007-2018	2018-2025
RC	Heavy+	5 (0.0%)	30 (0.1%)	1 (0.0%)	1 (0.0%)	0 (0.0%)
	MD	0 (0.0%)	7 (0.0%)	0 (0.0%)	0 (0.0%)	0 (0.0%)
	SD	50 (0.2%)	236 (1.1%)	13 (0.1%)	20 (0.1%)	6 (0.0%)
	ND	181 (0.8%)	2073 (9.5%)	311 (1.4%)	772 (3.5%)	353 (1.6%)
	No Eval.	69 (0.3%)	184 (0.8%)	17 (0.1%)	66 (0.3%)	90 (0.4%)
Masonry	Heavy+	308 (1.4%)	129 (0.6%)	9 (0.0%)	11 (0.1%)	0 (0.0%)
	MD	0 (0.0%)	1 (0.0%)	0 (0.0%)	0 (0.0%)	0 (0.0%)
	SD	898 (4.1%)	643 (2.9%)	24 (0.1%)	38 (0.2%)	5 (0.0%)
	ND	3675 (16.8%)	4724 (21.6%)	202 (0.9%)	344 (1.6%)	150 (0.7%)
	No Eval.	2855 (13.1%)	1105 (5.1%)	16 (0.1%)	50 (0.2%)	40 (0.2%)
Precast	Heavy+	0 (0.0%)	0 (0.0%)	0 (0.0%)	0 (0.0%)	0 (0.0%)
	MD	0 (0.0%)	0 (0.0%)	0 (0.0%)	0 (0.0%)	0 (0.0%)
	SD	60 (0.3%)	0 (0.0%)	0 (0.0%)	0 (0.0%)	1 (0.0%)
	ND	153 (0.7%)	53 (0.2%)	4 (0.0%)	51 (0.2%)	67 (0.3%)
	No Eval.	16 (0.1%)	21 (0.1%)	0 (0.0%)	22 (0.1%)	9 (0.0%)
Steel	Heavy+	0 (0.0%)	0 (0.0%)	0 (0.0%)	0 (0.0%)	1 (0.0%)
	MD	0 (0.0%)	0 (0.0%)	0 (0.0%)	0 (0.0%)	0 (0.0%)
	SD	0 (0.0%)	1 (0.0%)	0 (0.0%)	0 (0.0%)	0 (0.0%)
	ND	4 (0.0%)	15 (0.1%)	8 (0.0%)	45 (0.2%)	25 (0.1%)
	No Eval.	12 (0.1%)	2 (0.0%)	0 (0.0%)	3 (0.0%)	7 (0.0%)
Hybrid	Heavy+	20 (0.1%)	10 (0.0%)	1 (0.0%)	0 (0.0%)	0 (0.0%)
	MD	0 (0.0%)	0 (0.0%)	0 (0.0%)	0 (0.0%)	0 (0.0%)
	SD	82 (0.4%)	140 (0.6%)	2 (0.0%)	4 (0.0%)	1 (0.0%)
	ND	288 (1.3%)	689 (3.2%)	43 (0.2%)	81 (0.4%)	20 (0.1%)
	No Eval.	82 (0.4%)	89 (0.4%)	4 (0.0%)	5 (0.0%)	5 (0.0%)
ALL	Heavy+	333 (1.5%)	169 (0.8%)	11 (0.1%)	12 (0.1%)	1 (0.0%)
	MD	0 (0.0%)	8 (0.0%)	0 (0.0%)	0 (0.0%)	0 (0.0%)
	SD	1090 (5.0%)	1020 (4.7%)	39 (0.2%)	62 (0.3%)	13 (0.1%)
	ND	4301 (19.7%)	7554 (34.6%)	568 (2.6%)	1293 (5.9%)	615 (2.8%)
	No Eval.	3034 (13.9%)	1401 (6.4%)	37 (0.2%)	146 (0.7%)	151 (0.7%)

Note: Heavy+ = Collapse (C) + Urgent Demolition (UD) + Heavy Damage (HD); MD = Moderate Damage; SD = Slight Damage; ND = No Damage; No Eval. = not evaluated. Counts combine city center and rural survey areas.

Table 5: Damage level distribution by number of story in the rural areas for the 27 October 2025 Sındırgı earthquake (The second damaging earthquake of the sequence)

Structural System	Damage Level	0-2 stories	3-4 stories	5-7 stories
RC	Heavy+	8 (0.0%)	18 (0.1%)	11 (0.1%)
	MD	1 (0.0%)	6 (0.0%)	0 (0.0%)
	SD	155 (0.7%)	132 (0.6%)	38 (0.2%)
	ND	2855 (13.1%)	714 (3.3%)	121 (0.6%)
	No Eval.	345 (1.6%)	72 (0.3%)	9 (0.0%)
Masonry	Heavy+	449 (2.1%)	8 (0.0%)	0 (0.0%)
	MD	0 (0.0%)	1 (0.0%)	0 (0.0%)
	SD	1596 (7.3%)	11 (0.1%)	1 (0.0%)
	ND	9005 (41.2%)	88 (0.4%)	2 (0.0%)
	No Eval.	4045 (18.5%)	21 (0.1%)	0 (0.0%)
Precast	Heavy+	0 (0.0%)	0 (0.0%)	0 (0.0%)
	MD	0 (0.0%)	0 (0.0%)	0 (0.0%)
	SD	61 (0.3%)	0 (0.0%)	0 (0.0%)
	ND	327 (1.5%)	1 (0.0%)	0 (0.0%)
	No Eval.	68 (0.3%)	0 (0.0%)	0 (0.0%)
Steel	Heavy+	1 (0.0%)	0 (0.0%)	0 (0.0%)
	MD	0 (0.0%)	0 (0.0%)	0 (0.0%)
	SD	1 (0.0%)	0 (0.0%)	0 (0.0%)
	ND	92 (0.4%)	5 (0.0%)	0 (0.0%)
	No Eval.	24 (0.1%)	0 (0.0%)	0 (0.0%)
Hybrid	Heavy+	28 (0.1%)	3 (0.0%)	0 (0.0%)
	MD	0 (0.0%)	0 (0.0%)	0 (0.0%)
	SD	208 (1.0%)	21 (0.1%)	0 (0.0%)
	ND	1067 (4.9%)	54 (0.2%)	0 (0.0%)
	No Eval.	174 (0.8%)	10 (0.0%)	1 (0.0%)
ALL	Heavy+	486 (2.2%)	29 (0.1%)	11 (0.1%)
	MD	1 (0.0%)	7 (0.0%)	0 (0.0%)
	SD	2021 (9.2%)	164 (0.8%)	39 (0.2%)
	ND	13346 (61.1%)	862 (3.9%)	123 (0.6%)
	No Eval.	4656 (21.3%)	103 (0.5%)	10 (0.0%)

Note: Heavy+ = Collapse (C) + Urgent Demolition (UD) + Heavy Damage (HD); MD = Moderate Damage; SD = Slight Damage; ND = No Damage; No Eval. = not evaluated. Counts combine city center and rural survey areas.

Table 6: Damage level distribution by occupancy in the rural areas for the 27 October 2025 Sındırgı earthquake (The second damaging earthquake of the sequence)

Structural System	Damage Level	Stable	Storage	Residential	Public	Barn	Shop	Abandoned
RC	Heavy+	0 (0.0%)	1 (0.0%)	16 (0.1%)	0 (0.0%)	0 (0.0%)	20 (0.1%)	0 (0.0%)
	MD	0 (0.0%)	0 (0.0%)	2 (0.0%)	0 (0.0%)	0 (0.0%)	5 (0.0%)	0 (0.0%)
	SD	1 (0.0%)	10 (0.0%)	239 (1.1%)	1 (0.0%)	0 (0.0%)	74 (0.3%)	0 (0.0%)
	ND	8 (0.0%)	64 (0.3%)	3231 (14.8%)	18 (0.1%)	1 (0.0%)	366 (1.7%)	2 (0.0%)
	No Eval.	0 (0.0%)	9 (0.0%)	337 (1.5%)	0 (0.0%)	0 (0.0%)	73 (0.3%)	7 (0.0%)
Masonry	Heavy+	30 (0.1%)	18 (0.1%)	376 (1.7%)	0 (0.0%)	5 (0.0%)	23 (0.1%)	5 (0.0%)
	MD	0 (0.0%)	0 (0.0%)	1 (0.0%)	0 (0.0%)	0 (0.0%)	0 (0.0%)	0 (0.0%)
	SD	41 (0.2%)	47 (0.2%)	1467 (6.7%)	3 (0.0%)	6 (0.0%)	39 (0.2%)	5 (0.0%)
	ND	227 (1.0%)	339 (1.6%)	8163 (37.3%)	28 (0.1%)	38 (0.2%)	268 (1.2%)	32 (0.1%)
	No Eval.	65 (0.3%)	130 (0.6%)	3439 (15.7%)	6 (0.0%)	19 (0.1%)	90 (0.4%)	317 (1.5%)
Precast	Heavy+	0 (0.0%)	0 (0.0%)	0 (0.0%)	0 (0.0%)	0 (0.0%)	0 (0.0%)	0 (0.0%)
	MD	0 (0.0%)	0 (0.0%)	0 (0.0%)	0 (0.0%)	0 (0.0%)	0 (0.0%)	0 (0.0%)
	SD	0 (0.0%)	0 (0.0%)	61 (0.3%)	0 (0.0%)	0 (0.0%)	0 (0.0%)	0 (0.0%)
	ND	4 (0.0%)	13 (0.1%)	277 (1.3%)	0 (0.0%)	0 (0.0%)	30 (0.1%)	4 (0.0%)
	No Eval.	3 (0.0%)	3 (0.0%)	29 (0.1%)	1 (0.0%)	0 (0.0%)	11 (0.1%)	21 (0.1%)
Steel	Heavy+	0 (0.0%)	0 (0.0%)	0 (0.0%)	0 (0.0%)	0 (0.0%)	1 (0.0%)	0 (0.0%)
	MD	0 (0.0%)	0 (0.0%)	0 (0.0%)	0 (0.0%)	0 (0.0%)	0 (0.0%)	0 (0.0%)
	SD	0 (0.0%)	0 (0.0%)	0 (0.0%)	0 (0.0%)	0 (0.0%)	1 (0.0%)	0 (0.0%)
	ND	18 (0.1%)	27 (0.1%)	23 (0.1%)	1 (0.0%)	2 (0.0%)	25 (0.1%)	1 (0.0%)
	No Eval.	1 (0.0%)	12 (0.1%)	7 (0.0%)	1 (0.0%)	0 (0.0%)	3 (0.0%)	0 (0.0%)
Hybrid	Heavy+	0 (0.0%)	1 (0.0%)	27 (0.1%)	0 (0.0%)	0 (0.0%)	3 (0.0%)	0 (0.0%)
	MD	0 (0.0%)	0 (0.0%)	0 (0.0%)	0 (0.0%)	0 (0.0%)	0 (0.0%)	0 (0.0%)
	SD	1 (0.0%)	7 (0.0%)	198 (0.9%)	0 (0.0%)	1 (0.0%)	22 (0.1%)	0 (0.0%)
	ND	29 (0.1%)	41 (0.2%)	988 (4.5%)	0 (0.0%)	4 (0.0%)	58 (0.3%)	1 (0.0%)
	No Eval.	4 (0.0%)	3 (0.0%)	157 (0.7%)	1 (0.0%)	0 (0.0%)	10 (0.0%)	10 (0.0%)
ALL	Heavy+	30 (0.1%)	20 (0.1%)	419 (1.9%)	0 (0.0%)	5 (0.0%)	47 (0.2%)	5 (0.0%)
	MD	0 (0.0%)	0 (0.0%)	3 (0.0%)	0 (0.0%)	0 (0.0%)	5 (0.0%)	0 (0.0%)
	SD	43 (0.2%)	64 (0.3%)	1965 (9.0%)	4 (0.0%)	7 (0.0%)	136 (0.6%)	5 (0.0%)
	ND	286 (1.3%)	484 (2.2%)	12682 (58.0%)	47 (0.2%)	45 (0.2%)	747 (3.4%)	40 (0.2%)
	No Eval.	73 (0.3%)	157 (0.7%)	3969 (18.2%)	9 (0.0%)	19 (0.1%)	187 (0.9%)	355 (1.6%)

Note: Heavy+ = Collapse (C) + Urgent Demolition (UD) + Heavy Damage (HD); MD = Moderate Damage; SD = Slight Damage; ND = No Damage; No Eval. = not evaluated. Counts combine city center and rural survey areas.

3.4 Transition of damage states after the earthquake sequence

Evaluating damage-state transitions induced by the second damaging earthquake constitutes another critical parameter in understanding cumulative seismic effects. A total of 16,127 buildings were commonly inspected following both events. Among these, approximately 30% (4,872 buildings) exhibited a change in damage classification attributable to cumulative damage under successive seismic loading. Figure 11 presents the distribution of these buildings according to structural system and settlement type (urban vs. rural). The results indicate that nearly 84% of the buildings experiencing damage-state transitions are masonry structures. Moreover, the majority of these masonry buildings (4,070 cases) are located in rural areas. These findings clearly identify masonry construction, particularly in rural contexts, as the most vulnerable structural typology under consecutive earthquake scenarios. Figure 12 provides the conditional distribution of post-second-earthquake damage states as a function of the initial damage classification following the first event. The presented transition data in Fig. 12 reveal a pronounced cumulative damage effect across the Sındırgı doublet sequence. Buildings that sustained SD state in the first event escalated to HD in the second event at markedly higher rates (11.1% urban and 12.5% rural) compared with initial ND buildings, of which only 1.2% progressed to HD in both subsets. When escalation to heavy+ damage state is considered overall, SD-classified buildings escalate at roughly 13-15%, nearly an order of magnitude above the ~1.5% observed for ND buildings. Conversely, ND buildings display strong resilience, with 82.4% (urban) and 77.6% (rural) retaining an undamaged classification after the second event, indicating sufficient reserve capacity in structures without pre-existing damage; the non-negligible share reclassified as SD (7.8-9.0%) nonetheless shows that a "no-damage" outcome after the first shock does not preclude new damage initiation under the second. The three collapses recorded exclusively among initially ND-classified urban masonry buildings are also noteworthy despite their low frequency, as a solid proof of that sudden collapse in structures previously screened as undamaged may point to vulnerabilities that cannot be captured by visual screening after the first shock. Moreover, transitions from ND to SD and from SD to HD suggest that, in urban environments, damage tends to accumulate progressively and in stages rather than through abrupt structural deterioration. In contrast, rural areas display a distinctly different response pattern. Rural buildings initially categorized as ND or SD show a significantly greater tendency to transition directly into more severe damage states following the second earthquake. Beyond these, Fig. 12 demonstrates that damage evolution under successive earthquakes is not homogeneous across settlement types. Urban buildings generally exhibit more gradual damage accumulation, whereas rural buildings are characterized by sharper escalation of damage and reduced residual capacity under repeated seismic excitation. These empirical findings align with analytical and experimental studies indicating that even limited initial damage, such as micro-cracking, residual drifts, or bond deterioration, can substantially reduce stiffness and energy dissipation capacity, thereby increasing vulnerability to subsequent ground motions. Comparable patterns have been reported in previous earthquake sequences, where moderate aftershocks produced disproportionate damage in buildings previously classified as slightly damaged [1, 3-4, 30-31, 38-41].

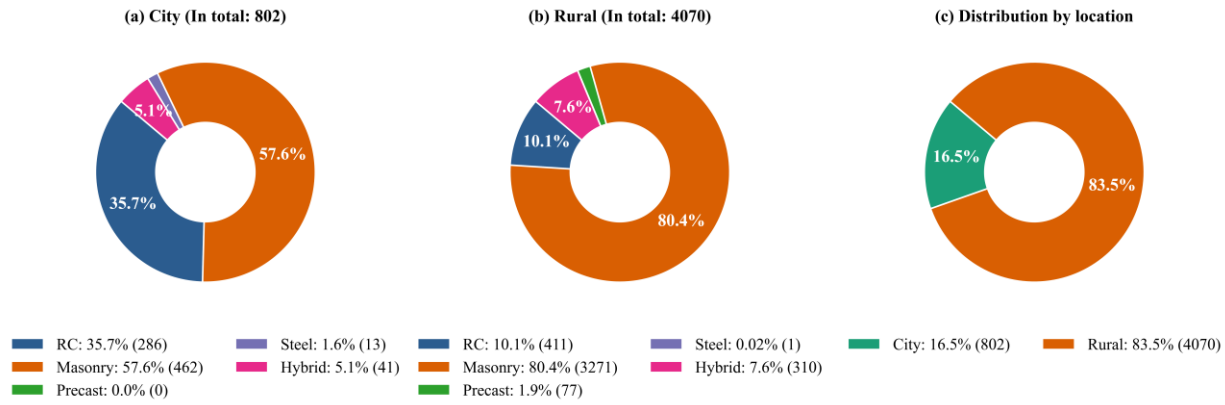

Figure 11: Distribution of structural systems for buildings whose damage state changed between the two earthquakes (10 August 2025 and 27 October 2025)

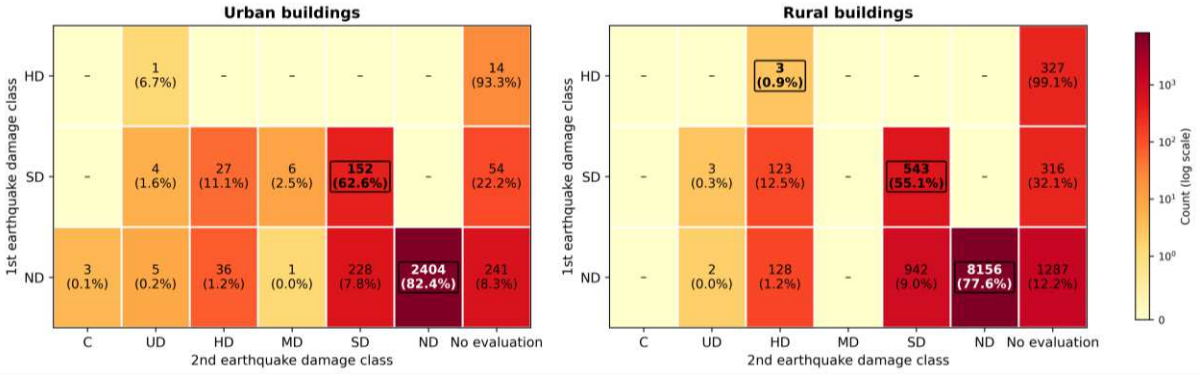

Figure 12: Damage class transition between successive earthquakes. Note: Cell values refer to the building count and their percentage, boxed values in cells show unchanged damage classes.

4 CASE STUDY BUILDINGS

Following the first earthquake in the Sındırgı sequence, a detailed field reconnaissance was conducted on 10 RC buildings in the city center to investigate the governing causes of the observed damage. Details about these 10 buildings are reported in an earlier paper [24]. Among these inspected buildings, two adjacent RC structures, B9 and B10, were selected for in-depth investigation due to their comparable height, construction period, and overall structural configuration, yet markedly different post-sequence seismic performance. While both buildings were classified as heavily damaged after the first earthquake, their response to the second event diverged significantly. Building B9 experienced a complete collapse during the 27 October 2025 earthquake, whereas Building B10 remained standing, albeit with aggravated structural damage (Figs. 13 and 14). This contrast provides a valuable basis for examining the role of cumulative damage, and local detailing deficiencies under repeated seismic excitation. The buildings were located approximately 900 m from the 1015 accelerometer station, which had a shear-wave velocity (Vs30) of 238 m/s [24], corresponding to ZD soil class according to TBEC 2018 [25]. Both buildings were constructed in the early 1990s with a partial basement,

a ground floor and four stories. Both are mixed-use RC frame structures, featuring commercial occupancy at the ground floor and residential units on the upper stories. Ground floor heights were greater than those of the upper floors in both buildings as well as ground floor having significantly lower amount of infill walls, suggesting a potential soft-story behavior under lateral loading. Neither structure incorporates shear walls; lateral resistance is provided exclusively by moment-resisting frames with beam-slab systems. On-site surveys included detailed measurements of plan geometry, story heights, column and beam layouts, and reinforcement detailing, complemented by non-destructive testing and material sampling/testing. At the time of their construction, these buildings were subject to the seismic design provisions in force in Türkiye during the early 1990s. The evolution of seismic design codes and the challenges associated with their implementation in existing buildings have been discussed by Ilki and Celep [47]; discrepancies between seismic design requirements and their actual implementation during construction stage have been an important concern for existing buildings in Türkiye. The substantial deficiencies identified in Buildings B9 and B10 may reflect similar shortcomings in construction practices and the implementation of seismic design provisions during their construction period.

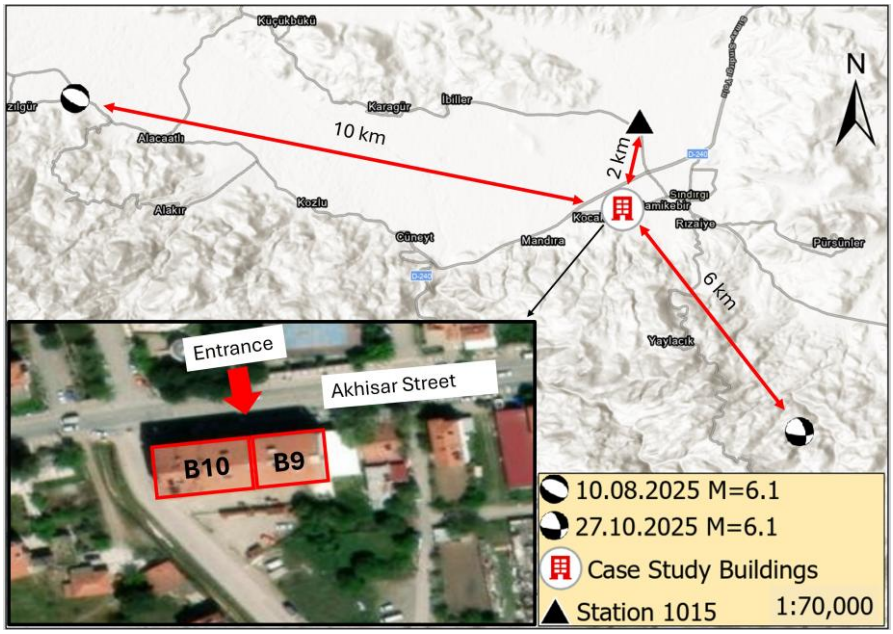

Figure 13: Locations of Buildings B9 and B10





a) b)



c) d)

Figure 14: a) Front view of Building B9 after the first earthquake, b) back view of Buildings B9 and B10 after the first earthquake, c) front view of Building B10 after the first earthquake, d) front view of the Building B10 after the second earthquake

The plan and elevation configurations of Buildings B9 and B10, derived from field measurements, are presented in Figs. 15 and 16, respectively. Both buildings exhibit relatively large ground-floor footprint areas, approximately 350 m² for B9 and 420 m² for B10, which were among the largest within the inspected building stock in Sındırgı. The increased mass associated with these large plan dimensions inherently attracted higher seismic forces, intensifying demand on vertical load-carrying elements. A critical geometric deficiency common to both buildings is the presence of undersized columns, particularly in one principal direction, where column depths were limited to 20-25 cm. These dimensions fall below the minimum requirements of the current Turkish Building Earthquake Code (TBEC 2018) [25] and significantly constrain axial, flexural, and shear capacities. Slender column proportions also exacerbate second-order (P–Δ) effects, increasing lateral displacements and internal force demands during seismic loading. Moreover, such slender sections may have caused compaction problems during concrete pouring as well as leading to drawbacks on reinforcement detailing. In addition to inadequate column dimensions, both buildings display pronounced plan and vertical irregularities. Irregular column grids with discontinuous axes disrupt uniform stiffness distribution and generate additional torsional effects. Moreover, heavy cantilever projections at the upper floors (Figs. 13 and 14) introduce additional gravitational and lateral displacement demands on supporting columns. These overhangs shift column axes between stories, creating vertical misalignments that compromise load transfer mechanisms and concentrate stresses in some of the members. In both B9 and B10 buildings, masonry infill walls were made of hollow clay bricks with 2-3 cm thick cementitious plaster. The infill walls were largely not present at the ground story to accommodate commercial use, while upper stories retain infilled frames associated with residential occupancy. This abrupt stiffness discontinuity in elevation results in a soft-story mechanism, leading to concentrated interstory drift demands at the ground story level.

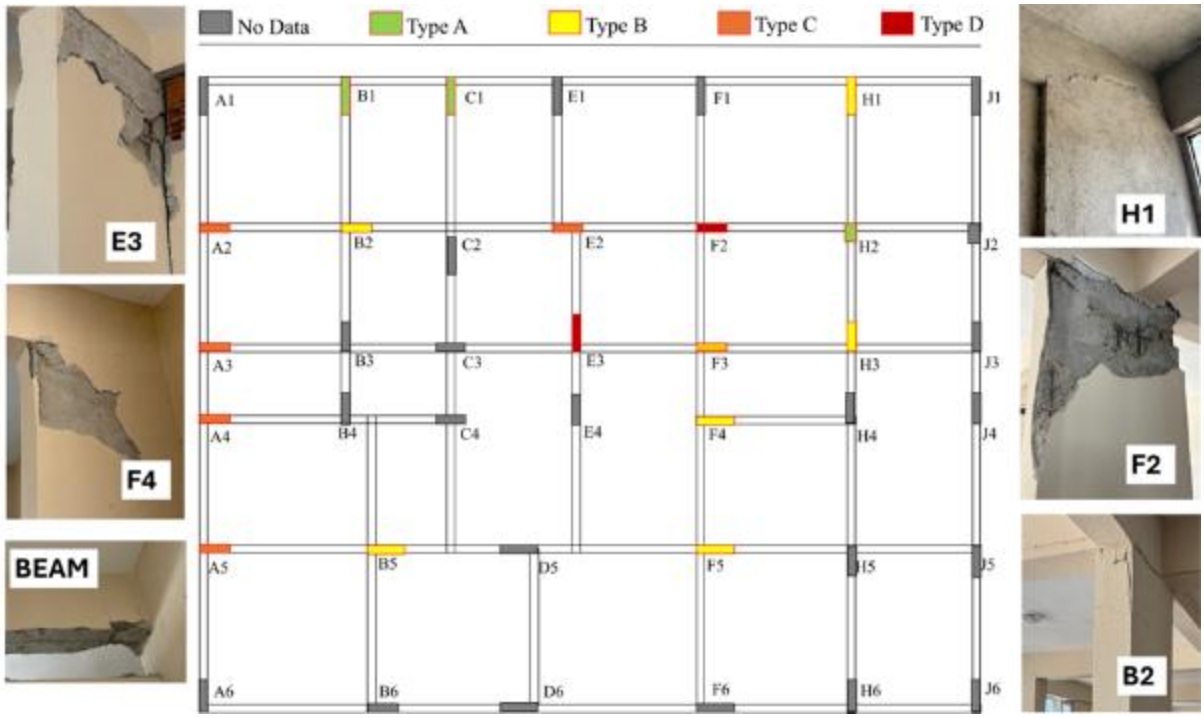

a)

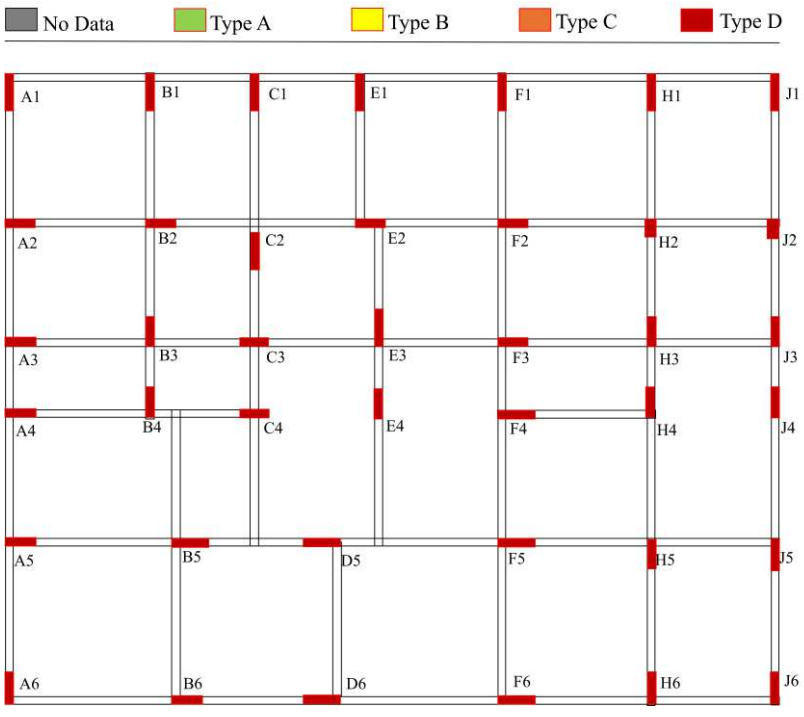

b)

Figure 15: Observed damages in Building B9 at ground floor, a) after the first earthquake, b) after the second earthquake (collapsed)

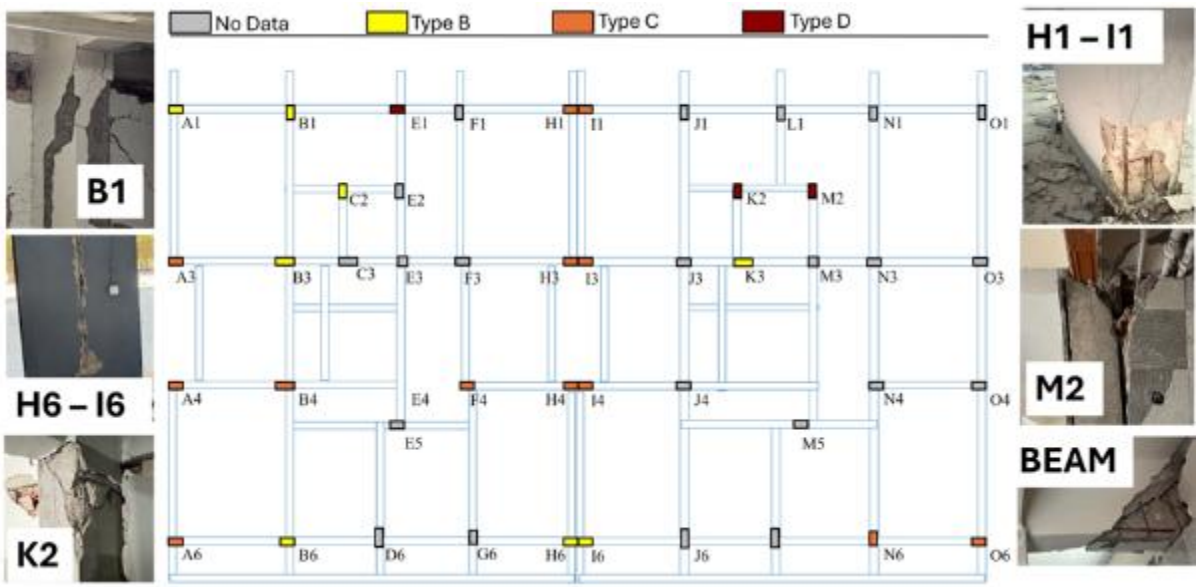

a)

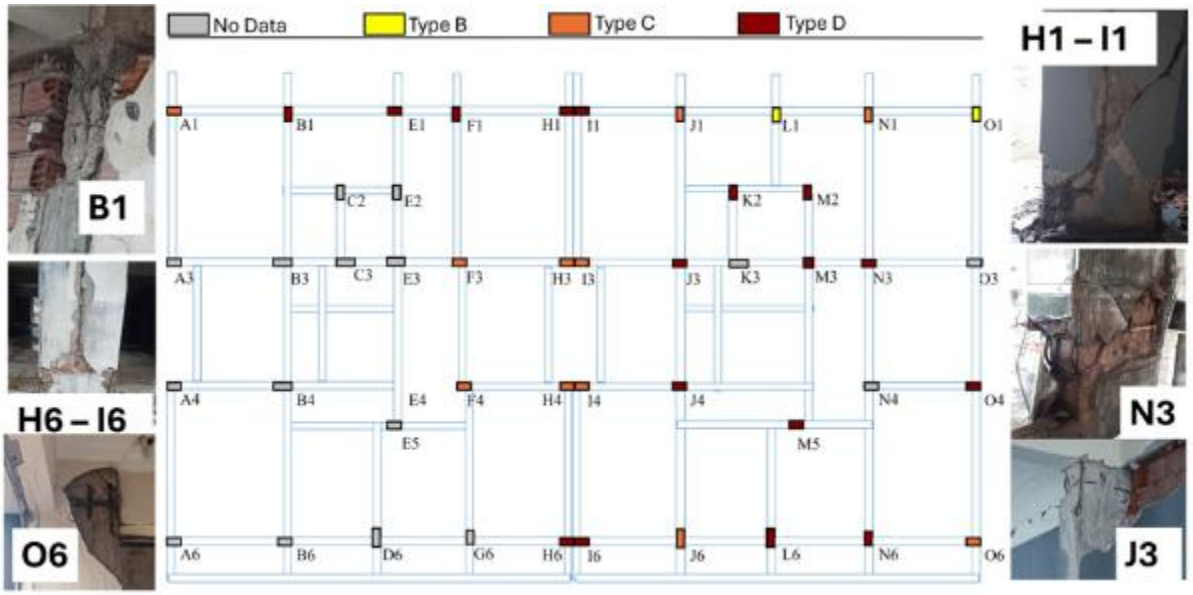

b)

Figure 16: Observed damages in Building B10 at ground floor, a) after the first earthquake, b) after the second earthquake

Material characterization revealed substantial deficiencies consistent with pre-2000 construction practices in the region. Average concrete compressive strength, determined through core testing, was around 6.8 MPa for B9 and 15.2 MPa for B10, indicating very poor material quality. Such low-strength concrete significantly reduces axial load capacity, stiffness, and energy dissipation capacity compared to the values considered in design, rendering the structures highly vulnerable to seismic demands. Reinforcement details for buildings B9 and B10 are summarized in Tables 7 and 8, respectively. Both buildings employed plain (non-

deformed) longitudinal reinforcement, which inherently provides inferior bond performance compared to deformed bars. The weak steel-concrete bond promotes premature bar slip, inefficient stress transfer, and reduced cyclic ductility. Transverse reinforcement detailing was also highly inadequate, consisting of 6 mm diameter plain stirrups, spaced at 200-300 mm, with 90° hooks. This detailing offers minimal confinement to the concrete core, lacks on preventing spalling under cyclic loading, and increases susceptibility to longitudinal bar buckling and brittle shear failures. Longitudinal and transverse reinforcement ratios were detected to be considerably greater in the B10 building compared to the collapsed B9 building (Tables 7-8). Beam-column joints in both buildings also lacked sufficient transverse reinforcement and anchorage lengths on beam longitudinal bars, further compromising force transfer and joint shear capacity. These cumulative material and detailing deficiencies substantially limited the deformation capacity of the structural system.

Table 7. Reinforcement details of columns of Building B9 at the ground floor

Column Name	Section Dimensions (cm)	Reinforcement Details (mm) (longitudinal - transverse)*	Reinforcement Drawing
A1, B1, C1, E1, F1, H1, J1, C2, F4, B5, D5, F5, D6, F6	80/20	10ϕ12 - ϕ6/200 (0.71-0.035)	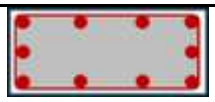
A2, B2, E2, F2, A3, B3, C3, E3, F3, H3, J3, A4, B4, C4, E4, H4, J4, A5, H5, J5, A6, B6, H6, J6	100/20	14ϕ12 - ϕ6/200 (0.79-0.028)	
H2, J2	50/30	10ϕ12 - ϕ6/200 (0.75-0.057)	

* Values in parenthesis refer to longitudinal and transverse reinforcement ratios, respectively)

Table 8. Reinforcement details of columns of Building B10 at the ground floor

Column Name	Section Dimensions (cm)	Reinforcement Details (mm) (longitudinal - transverse)	Reinforcement Drawing
A1, B1, F1, H1, E2, A3, E3, H3, A4, H4, A6, B6, I1, J1, L1, N1, O1, M2, I3, M3, I4, O6	45/25	8ϕ18 - ϕ6/200 (1.81-0.063)	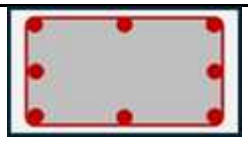
C2, F3, F4, E5, G6, H6, K2, J3, O3, J4, N4, O4, M5, I6, G6	45/25	8ϕ18 - ϕ6/200 (1.81-0.063)	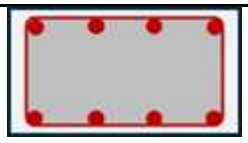

E1, N3	45/25	10ϕ18 - ϕ6/200 (2.26-0.063)	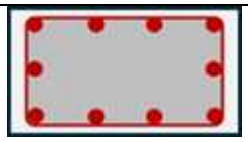
D6, J6, L6	55/25	8ϕ18 - ϕ6/200 (1.48-0.041)	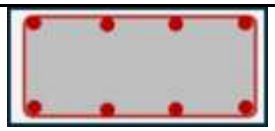
B3, B4	60/25	10ϕ18 - ϕ6/200 (1.69-0.047)	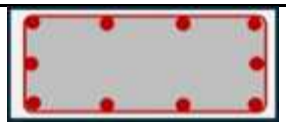
C3, K3	65/25	10ϕ18 - ϕ6/200 (1.57-0.044)	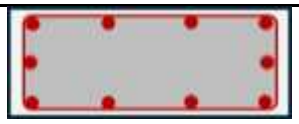

* Values in parenthesis refer to longitudinal and transverse reinforcement ratios, respectively)

For both B9 and B19 buildings, damage patterns observed after the first earthquake were primarily concentrated at the ground-story columns, consistent with the identified soft-story configuration. Column damage ranged from flexural cracking and cover spalling to severe shear cracking and crushing of concrete. Damage classifications for the columns are summarized in Figs. 15 and 16. After the second earthquake, Building B9 experienced progressive degradation resulting in total collapse. Field observations and subsequent evaluations suggest that the ground-story columns experienced a significant loss of residual axial and lateral load capacity due to cumulative damage, poor confinement, and material degradation (Figs. 15 and 16). Numerical analyses performed later in this study confirm that interstory drift demands at the first story exceeded critical thresholds during the second event. Building B10, despite exhibiting some material deficiencies, remained standing. Its relatively better material properties (i.e. higher concrete compressive strength, longitudinal and transverse reinforcement ratios compared to Building B9) along with more regular plan and elevation configuration, appear to have provided a certain extent of redundancy, preventing global collapse. Nevertheless, additional column and beam damage was documented after the second earthquake, indicating further degradation of stiffness and strength in the affected members. Localized reinforcement corrosion was observed in some columns along the exterior street-facing axes, associated with reduced concrete cover thicknesses of approximately 10-15 mm; interior columns exhibited comparatively less corrosion. Beam damage was also evident in both structures, particularly in short-span beams that were not fully framed between columns, where flexural cracking near column-beam joints suggested locally insufficient capacity. This localized damage may have contributed to a redistribution of internal forces among adjacent members.

The detailed documentation of geometry, material properties, and observed damage in Buildings B9 and B10 establishes a critical foundation for the numerical modeling presented in the following chapter. The pronounced deficiencies in column dimensions, material quality, reinforcement detailing, and geometric regularity, combined with cumulative damage from

successive earthquakes, are explicitly incorporated into the analytical models to realistically capture stiffness degradation, strength loss, and collapse mechanisms under repeated seismic loading.

4.1 Modelling

The case study buildings were numerically modelled using SeismoStruct [42] software to simulate the earthquake sequence. Cyclic behavior is defined through the material models. The nonlinear model for the existing confined concrete material is defined according to Mander et al. [43] (Fig. 17a). For the plain S220 steel reinforcement, the cyclic model introduced by Menegotto and Pinto [44] is assigned to the relevant section fibers (Fig. 17b). The SeismoStruct software assigns the nonlinearity to the section through section fibers. A representative section that demonstrates the section subdivision is given in Fig. 17c. Beams and columns were modelled as plastic hinge frame elements with an assumption of plastic hinges occur. As the plastic hinge length, half of the cross-section depth was defined for all elements. Rigid column-beam connections were used in the structural model since the observed seismic damage mostly occurred on the columns. The assigned modulus of elasticity for the concrete was determined using Eq. (2), where f_{cm} is the compressive strength of the existing concrete. For the infill walls, assigned compression and shear struts and their cyclic behaviors are illustrated in Fig. 17d. The drift ratio capacity of the infill walls in the case-study building was assumed to be approximately 0.5%, consistent with the drift limit specified for buildings containing brittle infill walls in certain design codes [46]. The compressive strength of the infill masonry was set to 1 MPa, while its elastic modulus was estimated as 600 times its compressive strength. However, the mechanical characteristics and failure behavior of masonry infill walls in RC frame buildings in Türkiye can differ considerably depending on construction workmanship, material quality, and interaction with the surrounding RC frame. Accordingly, the selected parameters are intended to represent plausible properties for the building under investigation and should not be regarded as precise, site-specific material characteristics. Following these modelling principles, the numerical models of the Building B9 and B10 were prepared (Fig. 17e-f). Fixed supports were assigned at the column bases because no foundation deformation or damage was observed during the field investigations. Rigid diaphragms were assigned at each floor level after modelling the slabs. In addition to the self-weight of the slabs, a superimposed dead and live loads of 1.5 kN/m^2 and 2.0 kN/m^2 were assigned to the slabs, respectively. The seismic mass was calculated by considering the full dead load and 30% of the live load, in accordance with the provisions of TBEC [25].

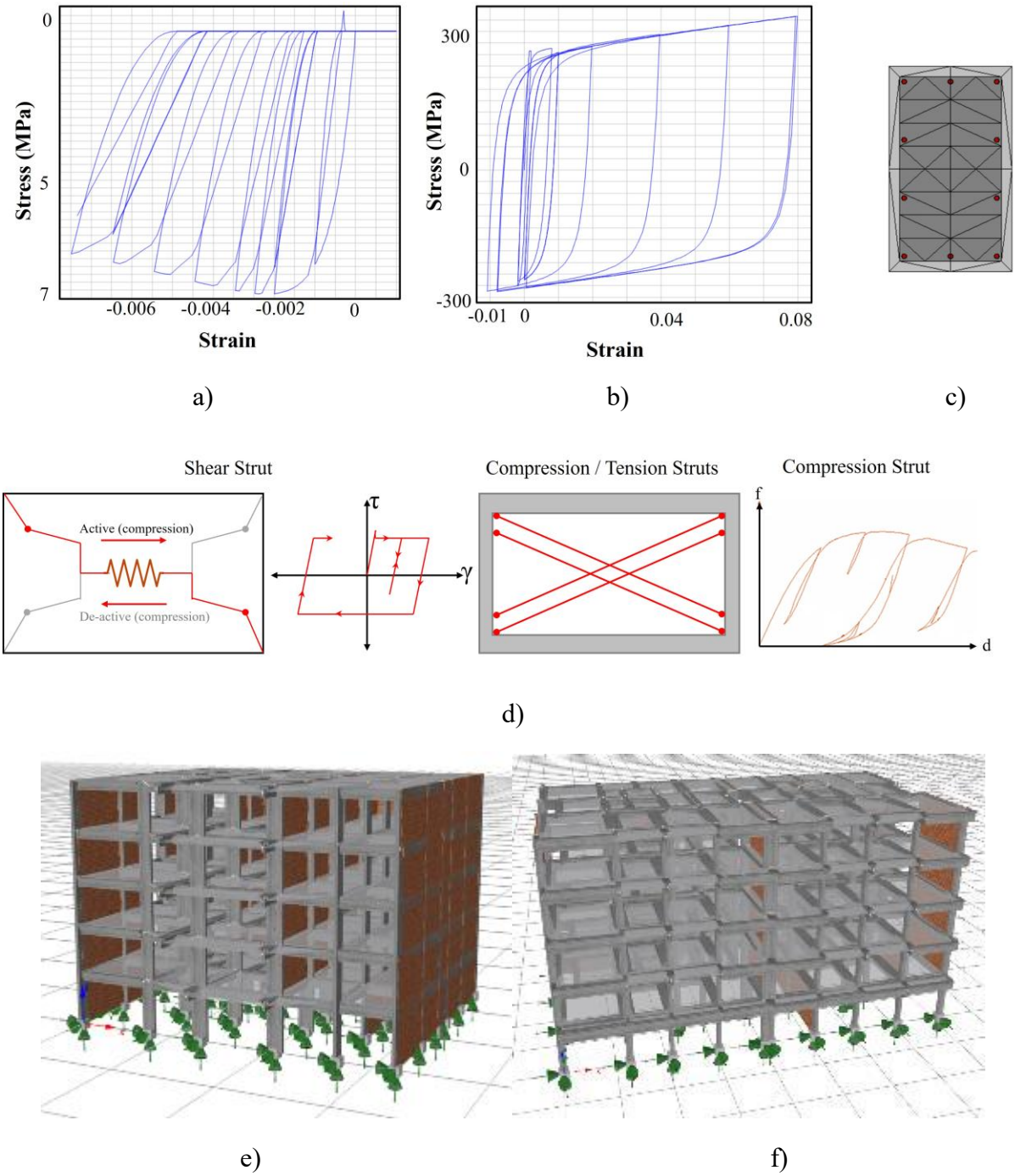

Figure 17: Stress-strain diagrams and cyclic behavior of a) concrete for Building B9, b) steel, c) section fibers of a representative column, d) configuration of shear and compression/tension struts of infill walls and used cyclic behavior, e) numerical model of the Building B9, f) numerical model of the Building B10

$$E_c = 5000\sqrt{f_{cm}} \tag{2}$$

To simulate the earthquake sequence, five significant ground motions (Fig. 1) were considered in the nonlinear time-history analyses. Following the initial M_w 6.1 event, M_w 5.0, M_w 4.8, M_w 5.0, and the final M_w 6.1 earthquake records were sequentially applied. The E–W, N–S, and

U–D components of the acceleration–time histories from station ID 1015 used in the analysis are presented in Fig. 1. Later, the consistency between the performance results of the RC elements obtained from numerical analyses and the damage classification outlined in Figs. 15 and 16 is evaluated using the limits illustrated in Fig. 18. In this approach, Damage Type D corresponds to the ultimate plastic rotation limit defined by TBEC [25] (Eq. 3). Damage Type C is taken as the rotation limit associated with the controlled damage state, defined as 75% of the ultimate plastic rotation. Damage Type B represents the yield rotation, calculated using Eq. (4). Finally, half of the yield rotation is adopted as the threshold for Damage Type A. Here, θ_y is the yield rotation, θ_u is the plastic rotation limit, $\emptyset_u$ is the ultimate curvature, $\emptyset_y$ is the yield curvature, L_p is the length of the plastic hinge, L_s is the shear span as the half of the clear height of the column or the half of the clear length of the beam, d_b is the average longitudinal reinforcement diameter at the tension zone. The shear strength of RC sections are also determined through Eq. (5) to 7), where V_r is the shear strength of the section, V_c and V_w is the contribution of concrete and transverse reinforcement to the shear strength of the section, N_k is the normal force, A_c is the cross-sectional area of the concrete core, b and d is the section width and depth, γ is the axial load coefficient (0.07 for axial compression and -0.3 for axial tension), s is the stirrup spacing, f_{ywn} and A_{sh} is the yield strength and area of the transverse reinforcement, respectively.

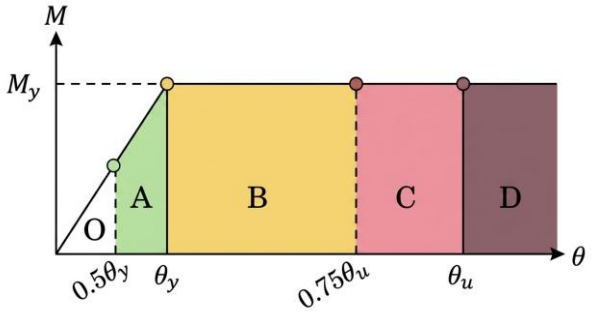

Figure 18: Chord rotation to seismic damage class conversion procedure

$$\theta_u = [(\emptyset_u - \emptyset_y)L_p\left(1 - 0.5\frac{L_p}{L_s}\right) + 4.5\emptyset_u d_b \quad (3)$$

$$\theta_y = \frac{\emptyset_y L_s}{3} + \frac{0}{0015\eta}\left(1 + 1.5\frac{h}{L_s}\right) + \frac{\emptyset_y d_b f_{ye}}{8\sqrt{f_{ce}}} \quad (4)$$

$$V_r = 0.8 \times V_c + V_w \quad (5)$$

$$V_c = 0.65(0.35\sqrt{f_{cm}})bd\left[1 + \gamma\frac{N_k}{A_c}\right] \quad (6)$$

$$V_w = \frac{A_{sh}}{s} f_{ywn} d \quad (7)$$

5 RESULTS AND DISCUSSION

Nonlinear time-history analyses were performed for the case-study buildings following the modelling approach described in Section 4.1. Each building was analysed both with and

without infill walls to compare their effects on structural response during the earthquake sequence. The results for Buildings B9 and B10 are presented in the following subsections.

5.1 Damage Evaluation without Infill Walls

Building B9 experienced heavy structural damage after the first earthquake and ultimately collapsed following the second earthquake in the sequence. Fig. 19a presents the shear demand-to-capacity ratio for a representative column (F2). The evolution of this ratio throughout the sequence indicates that the aftershocks (occurring between 50th and 110th seconds) did not significantly increase the damage in the structure. Fig. 19b illustrates the corresponding chord rotation demand time history for the same column. The chord rotation demand caused by the last earthquake was significantly larger than that of the first earthquake due to the degradation caused by the seismic damage. According to the numerical analysis, the building collapses during the second Mw 6.1 earthquake. It should be noted that the building is assumed to collapse either when all columns reach ultimate rotation capacities or the numerical analysis indicates a loss of structural stability.

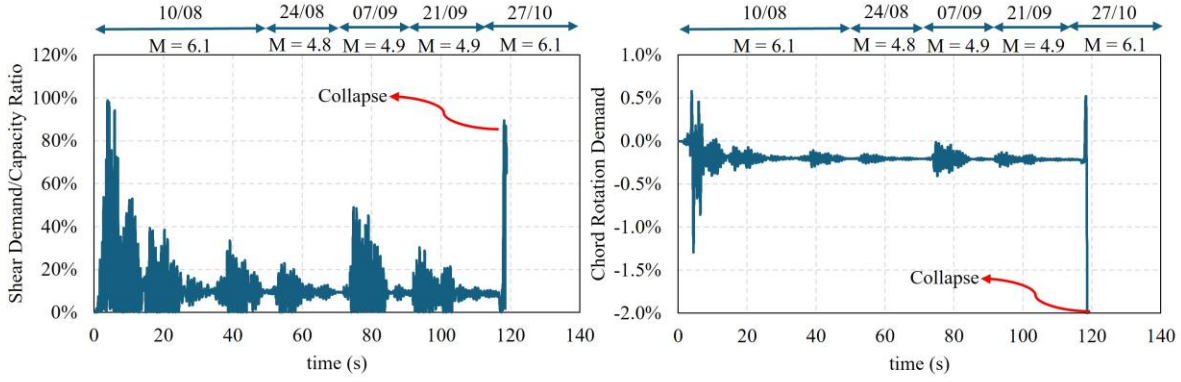

a) b)

Figure 19: a) Shear demand/capacity ratio, b) chord rotation demand time histories of F2 column during the earthquake sequence

It is also worth noting that, to incorporate the effects of damage states observed after the first earthquake into the numerical models, stiffness and strength modification coefficients were assigned to each damage type during the analysis, as summarized in Table 9 based on FEMA 306 [45]. As a result of this procedure, the shift in the fundamental periods of Building B9 is presented in Fig. 20. As shown in this figure, the spectral acceleration corresponding to the initial fundamental period was around 0.40g in the X direction and 0.60g in the Y direction. Following the first earthquake, the fundamental period increased from 0.52 s to 0.84 s in the X direction and from 0.46 s to 0.66 s in the Y direction due to the accumulated damage. This period shift directly modified the spectral acceleration demand during the subsequent earthquake, resulting in a 103% increase in the X direction and a 28% decrease in the Y direction relative to the demand imposed by the first earthquake.

Table 9: Stiffness and strength modification coefficients according to FEMA 306 [45]

Damage Type	Modification Coefficient		
	Stiffness	Strength	Ductility
O	1.0	1.0	1.0
A	0.6	1.0	1.0
B	0.5	0.8	0.9
C	0.2	0.3	0.7
D	0.0	0.0	0.0

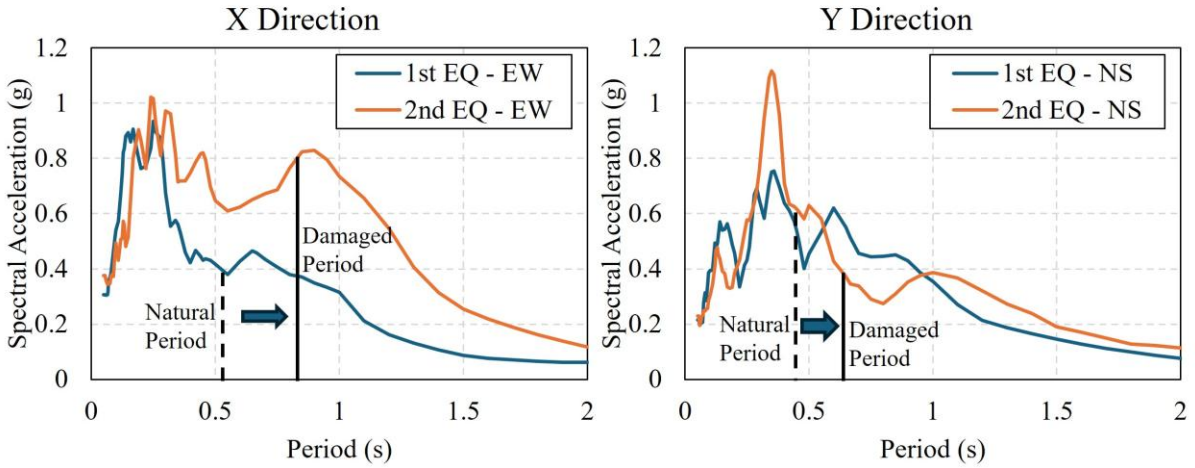

Figure 20: Damage induced shift in the spectral acceleration demand and fundamental periods of Building B9

The maximum chord rotation demand-to-capacity ratios (calculated using Eq. 3) for all columns during the first and second Mw = 6.1 earthquakes are presented in Fig. 21a. According to the numerical analysis results, the demands induced by the first event cause type D damage in several columns, while the remaining elements experienced widespread damage within the type B to type C range. During the second earthquake, the already weakened structural system was subjected to substantially higher chord rotation demands, ultimately leading to collapse. Fig. 21b illustrates the shear demand-to-capacity ratios for the first earthquake. The results indicate that nearly all columns exhibit shear-critical or flexure-shear behavior, which is consistent with the field observations.

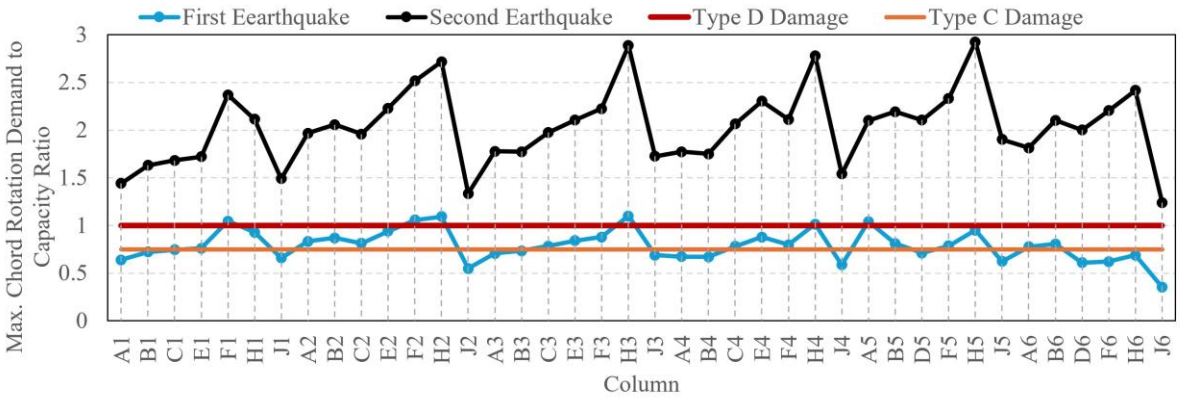

a)

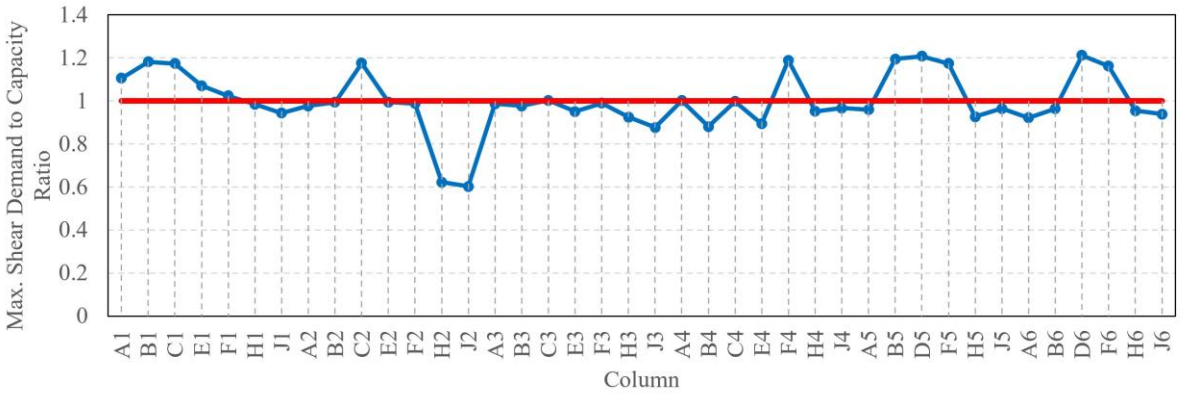

b)

Figure 21: Nonlinear time history analysis results for Building B9: a) column chord rotations, b) maximum column shear demands in the X and Y directions during the first earthquake (red line is the capacity limit)

Similar to Building B9, Building B10 experienced heavy structural damage during the first earthquake. However, unlike Building B9, this building was able to remain standing throughout the entire earthquake sequence. The level of seismic damage, nevertheless, increased considerably after the final event (the second Mw = 6.1 earthquake). Fig. 22a presents the shear demand-to-capacity ratio for a representative column (E1). As in the previous case, the intermediate aftershocks did not cause a significant increase in damage, as their shear demands were much lower than those induced by the Mw = 6.1 earthquakes. Fig. 22b displays the corresponding chord rotation demand time history for the same column. Although the chord rotation demand during the second Mw = 6.1 earthquake is noticeably higher than that of the first, the increase remains limited compared to the increase in demands observed in Building B9. Following the earthquake sequence, the structure sustained extensive seismic damage, and large residual displacements were identified in the numerical analysis.

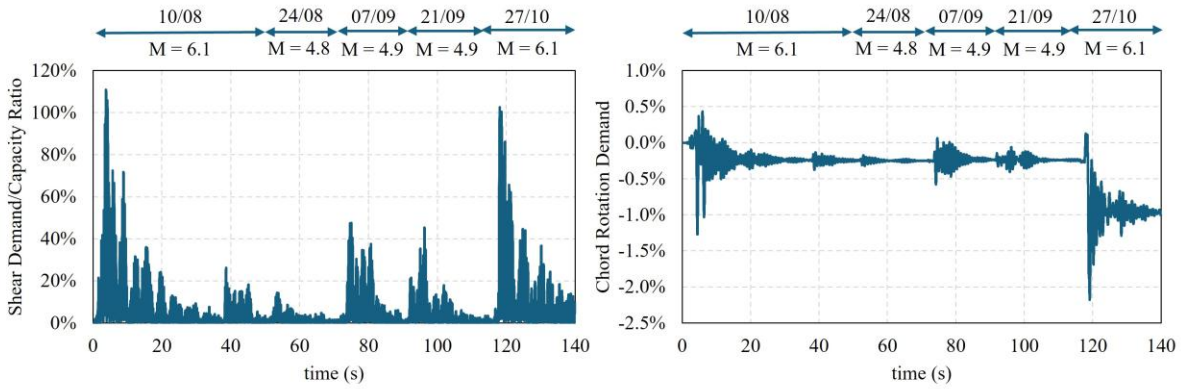

a) b)

Figure 22: a) Shear demand/capacity ratio, b) chord rotation demand time-histories of E1 column during the earthquake sequence

Fig. 23 illustrates the shift in the fundamental periods of Building B10 caused by structural damage during the first M_w 6.1 earthquake and the subsequent aftershocks, before the second M_w 6.1 earthquake. The fundamental period increased from 0.37 s to 0.52 s in the X direction and from 0.47 s to 0.65 s in the Y direction. As shown in Fig. 23, in the X direction, the damaged fundamental period of Building B10 coincided with a local minimum in the acceleration response spectrum of the second M_w 6.1 earthquake, whereas the initial fundamental period of Building B9 corresponded to a local peak (Fig. 20). Consequently, due to the differences in their dynamic characteristics, Building B9 was subjected to approximately 30% higher spectral acceleration demand than Building B10 during the second earthquake.

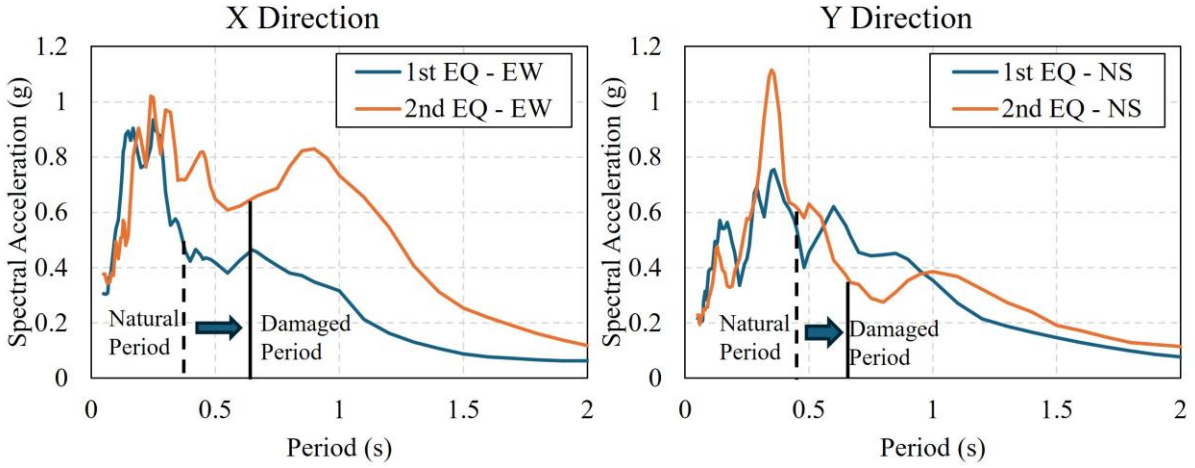

Figure 23: Damage induced shift in the spectral acceleration demand and fundamental periods of Building B10

The maximum chord rotation demand-to-capacity ratios (computed using Eq. 3) for all columns during the first and second Mw = 6.1 earthquakes are shown in Fig. 24a, while Fig. 24b presents the corresponding shear demand-to-capacity ratios for the first earthquake. The chord rotation demands resulting from the first earthquake yielded type C and type B damage for most columns, whereas four columns experienced shear force demands exceeding their shear

capacities, indicating shear failure. Similar to the Building B9, columns are likely to exhibit shear critical or flexure-shear behavior. Following the second earthquake, the majority of the columns exceeded the type D damage threshold. For seven columns, the maximum chord rotation demand-to-capacity ratio surpassed 1.25, and the demands on the remaining columns were close to the boundary between type C and type D damage.

The exceedance of the calculated shear capacity does not necessarily indicate imminent global collapse. The code-based equations used to estimate column shear capacity may incorporate a certain degree of conservatism. Furthermore, considering the attainment of the calculated shear capacity as the onset of shear failure is itself a conservative assumption, as it does not necessarily imply an immediate loss of the column's vertical load-carrying capacity or the occurrence of global structural collapse. A similar consideration applies to the chord rotation limits. The adopted limits, which are based on those used in the design of new buildings, incorporate safety margins and should not be interpreted as deterministic thresholds for structural collapse. Therefore, exceeding the chord rotation limit associated with Type D damage does not necessarily mean that the building will collapse.

This distinction is also reflected in the comparison between Buildings B9 and B10. In Building B9, the chord rotation demands reached approximately three times the ultimate limits (Fig. 21a), and the building collapsed during the second earthquake. In contrast, for Building B10, the maximum chord rotation demand-to-capacity ratio exceeded 1.50 in only one column and 1.25 in eight columns, while the demands in the remaining columns were close to the capacity limit (Fig. 24a). Considering the safety margins inherent in the adopted capacity limits, the relatively limited extent of these exceedances may partly explain why Building B10 did not collapse despite several columns exceeding their prescribed chord rotation capacities. These findings highlight that the exceedance of individual component-level capacity limits should be interpreted in conjunction with the extent and distribution of damage throughout the structural system when evaluating the likelihood of global collapse.

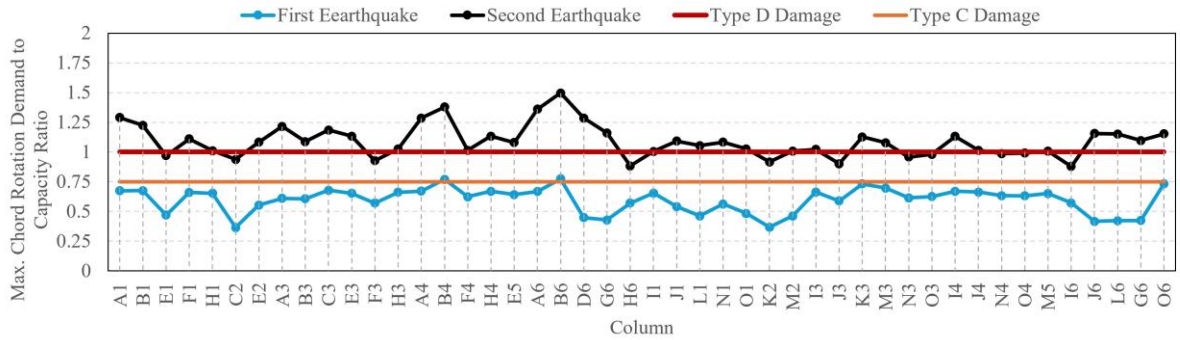

a)

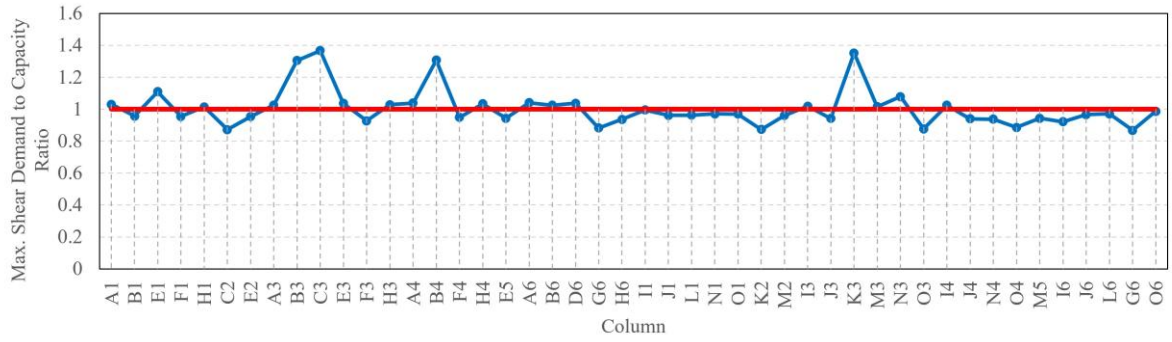

b)

Figure 24: Nonlinear time history analysis results for Building B10: a) column chord rotations, b) maximum column shear demands in the X and Y directions during the first earthquake (red line is the capacity limit)

Both buildings exhibited soft-story behavior due to the partial absence of infill walls at the ground story compared to the upper stories, resulting in damage concentrated in the entrance story columns. This behavior is reflected in the story displacement profiles shown in Fig. 25, which present the floor displacements at the instant of peak roof displacement during the first M_w = 6.1 earthquake. In both buildings, the displacement profiles indicate a pronounced concentration of lateral deformation at the entrance story, consistent with the observed damage patterns.

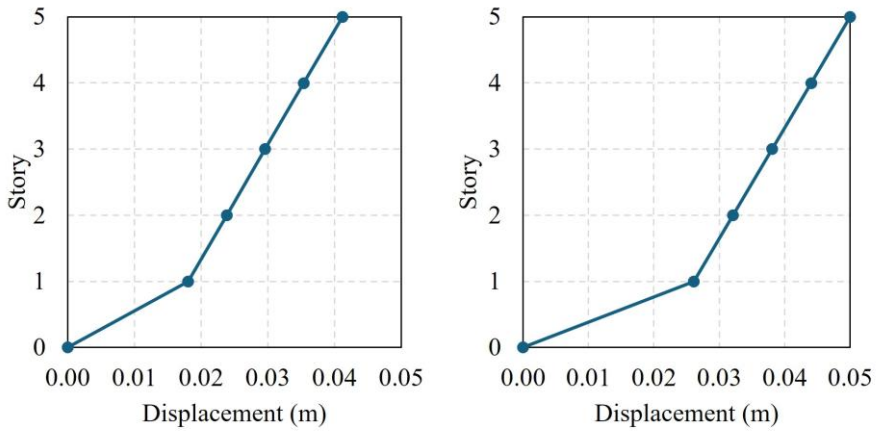

a) b)

Figure 25: Story displacement profile at peak roof displacement moment during the first Mw=6.1 earthquake: a) Building B9, b) Building B10

5.2 Effects of Infill Walls

With an aim to determine a more realistic behavior of the buildings, infill walls were also involved into the models. For Building B9, the presence of infill walls reduced the maximum first story displacement by 33% during the first earthquake and decreased the residual displacement by 42% (Fig. 26a). Nevertheless, the building collapsed by losing its stability in both modeling approaches. In Building B10, the infill walls similarly reduced the maximum first story displacement by 90% during the first earthquake and decreased the residual

displacement by 86% until the last earthquake (Fig. 26b). In addition, the model with infill walls experienced 31% lower first story displacement during the second Mw 6.1 event with respect to the model without infill walls, whereas the model without infill walls collapsed at the end of the earthquake sequence. The hysteretic responses of representative wall sections for both buildings are illustrated in Fig. 27.

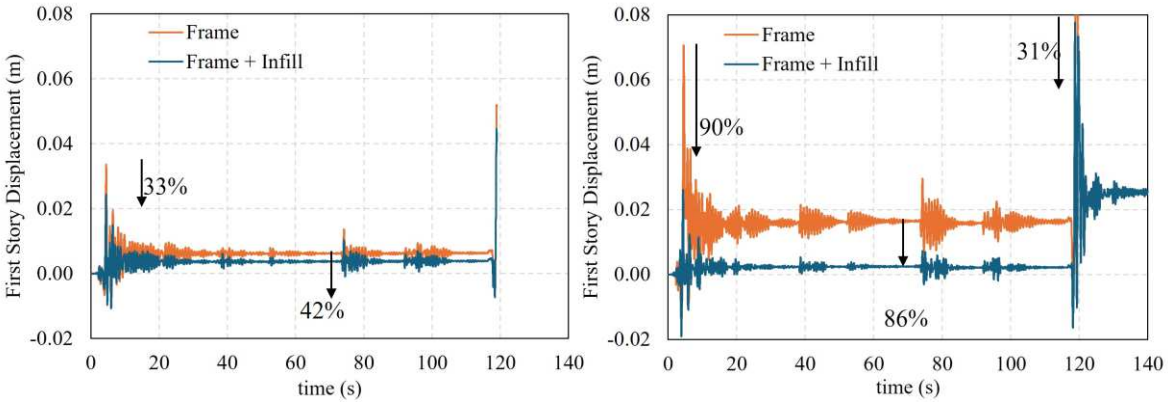

a) b)

Figure 26: Roof displacement time histories for both buildings, considering bare frame and frame+infill wall systems: a) Building B9, b) Building B10

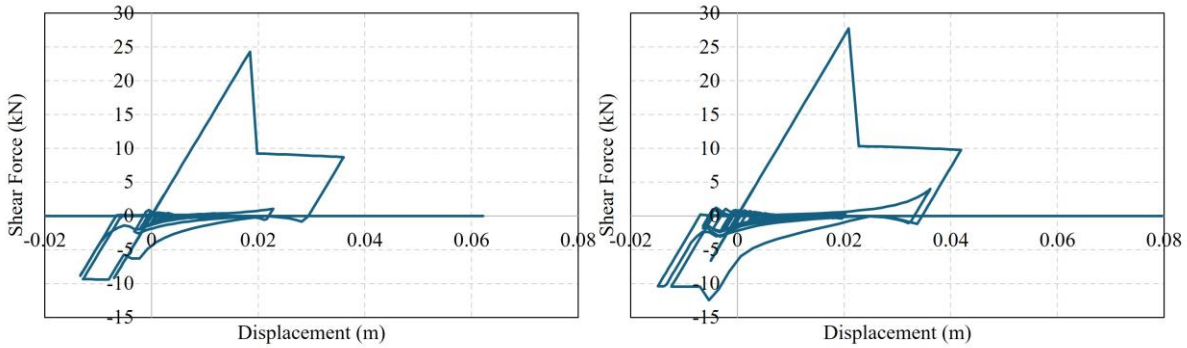

a) b)

Figure 27: Hysteretic curves of infill walls: a) the wall between columns A5 and A6 at the first story in Building B9, b) the wall between columns A4 and A6 at the first story in Building B10

The damage evaluation of both buildings was conducted considering both with and without infill wall models. Damage types of the columns were assigned based on the assumption shown in Fig. 18. Subsequently, the WDPVM value (Eq. 1) of each building after the first and second Mw = 6.1 earthquakes was determined using Eq. (1). The estimated global building damage levels are presented in Fig. 28. All modeling cases indicated heavy damage in both buildings after the first earthquake, which aligns well with the post-earthquake damage assessment results. Nevertheless, the calculated WDPVM values were somewhat higher than the damage levels observed in the field. This difference may partly be attributed to the conservatism inherent in the adopted component-level capacity limits, as discussed above. For Building B9,

the model without infill walls yielded a higher WDPVM value compared to the model with infills after the first earthquake. After the second earthquake, all RC columns in both models with and without infill walls reached damage type D. For Building B10, the presence of infill walls resulted in significantly lower WDPVM values after the first M_w = 6.1 earthquake. Following the second M_w = 6.1 event, all RC columns in the model without infill walls reached the type D damage state; however, a limited number of columns in the model with infill walls remained below the type D threshold after the entire earthquake sequence. In each case for both buildings, models without infill walls exhibited higher WDPVM values, indicating more severe damage.

The presence of infill walls probably reduced the WDPVM of Building B9 during the first earthquake, though the structure collapsed during the second event. This outcome was also captured by numerical analyses. For Building B10, both models, with and without infill walls, remained standing after the first earthquake. However, the model without infill walls collapsed during the second event, and the model with infill walls reached nearly collapse. The somewhat higher WDPVM values compared with the observed damage should be interpreted in light of the conservative assumptions underlying the adopted component-level damage limits. Exceeding these limits does not necessarily imply immediate global collapse, as the relationship between component-level damage and overall structural performance also depends on the extent and distribution of damage throughout the building. These results highlight that infill walls can mitigate the collapse of substandard buildings subjected to earthquakes with relatively short significant durations. However, if the significant duration of the shaking is longer, the numerical analysis considering the earthquake sequence indicates that infill walls fail at certain point, and frame starts to resist the seismic action.

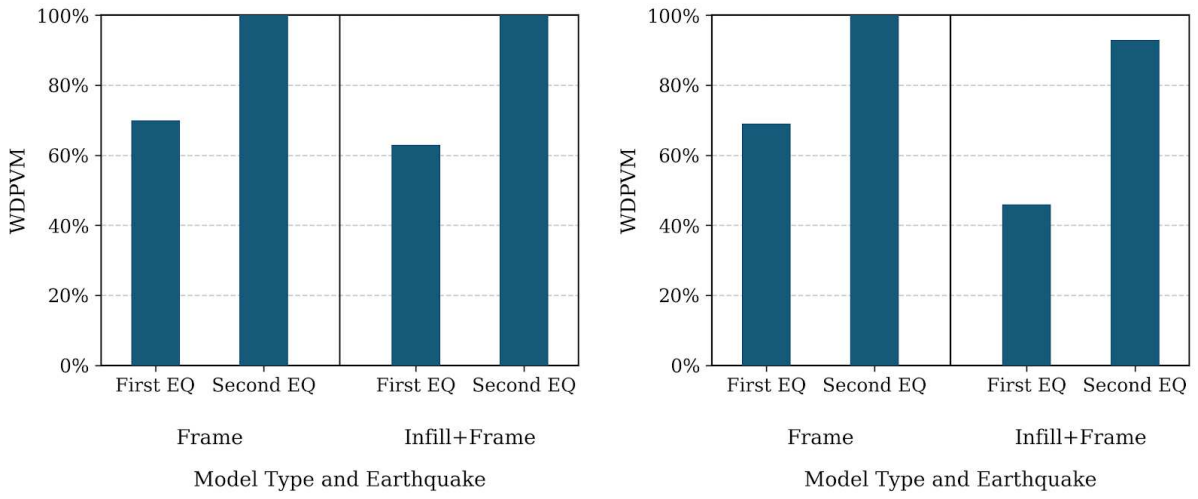

Figure 28: WDPVM for bare frame and frame+infill models after both earthquakes: a) Building B9, b) Building B10

6 CONCLUSIONS

This study presents an integrated assessment of the Sındırgı earthquake sequence to clarify how structural damage accumulates and residual capacity degrades under successive seismic events. Seismological analyses, comparative post-earthquake damage statistics, and detailed case studies of two reinforced concrete buildings (B9 and B10) are combined with nonlinear time-history modeling to quantify the influence of geometric deficiencies, material degradation, and pre-existing damage on structural performance during repeated earthquakes. The combined evaluation led to the following key conclusions:

1. After the first earthquake, about 95% of severe damage occurred in older stock, while post-2000 buildings showed markedly better performance, with no collapses and around 90% remaining undamaged after the second event. RC systems outperformed masonry, and public buildings were more resilient than residential and rural auxiliary structures.

2. Approximately 30% of commonly inspected buildings after both earthquakes experienced damage-state transitions between the two events, predominantly within older masonry stock. The results confirm cumulative damage effects and highlight the need to incorporate sequential earthquake scenarios into post-event assessment and retrofit prioritization.

3. Despite being subjected to similar seismic input, the observed damage variability within the inspected building stock, and particularly between buildings B9 and B10, was controlled by inadequate column dimensions, poor concrete quality, lack of ductility, insufficient transverse reinforcement detailing, and pronounced plan and vertical irregularities.

4. Numerical analyses demonstrated that while intermediate aftershocks ($Mw \leq 5.0$) caused limited incremental damage, the second earthquake imposed substantially higher chord rotation demands on already weakened structural systems. In Building B9, this cumulative degradation led to loss of axial and lateral load-carrying capacity at the ground story and ultimately resulted in collapse, whereas Building B10 retained marginal residual stability.

5. Although both buildings exhibited similar material deficiencies, Building B9 showed more severe irregularity-induced demand concentrations and higher rotation demand amplification due to dynamic properties. Building B10, despite experiencing extensive damage, benefited from a comparatively lower seismic spectral acceleration demand. Furthermore, during the second earthquake, Building B9 was subjected to approximately 30% higher spectral acceleration demand than Building B10, which may have further contributed to the difference in their seismic responses.

6. Shear-critical and flexure-shear failure mechanisms dominated the seismic response. Both field observations and numerical results consistently indicated that most columns operated in shear-critical or flexure-shear regimes due to low concrete strength, wide stirrup spacing, and inadequate confinement. This behavior resulted in brittle damage

accumulation and rapid degradation of deformation capacity, particularly after the first major event.

7. The inclusion of infill walls to numerical models reduced peak and soft first story displacements by up to 42-86% and delayed collapse in several scenarios. For Building B10, the analyses indicated that infill walls prevented collapse during the second earthquake, whereas the bare-frame model was predicted to collapse under the same event. However, when the entire earthquake sequence was considered, the infill walls progressively lost their load-carrying capacity as damage accumulated. Consequently, seismic demands were increasingly transferred to the RC frame, leading to further structural damage and bringing the building close to collapse.
8. The evolution of chord rotation demands, shear demand-to-capacity ratios, and weighted damage percentages for the columns closely matched the documented damage states after both earthquakes, confirming the suitability of rotation-based damage conversion procedures for evaluating cumulative seismic damage in substandard RC buildings.

Overall, the findings highlight that post-earthquake safety assessments and collapse predictions should explicitly consider earthquake sequences, cumulative damage effects, and the contribution of infill walls, rather than relying solely on single-event analyses or models that neglect infill wall behavior. In particular, substandard RC buildings with poor material properties and detailing may remain only moderately or slightly damaged after an initial earthquake but may still be unable to withstand subsequent strong earthquakes. These results have direct implications for rapid post-earthquake decision-making, emphasizing the need for conservative occupancy restrictions and timely intervention in heavily damaged RC building stocks subjected to ongoing seismic activity.

Acknowledgements

This study was supported by DASK (Turkish Catastrophe Insurance Pool) under the project entitled “Seismic Performance Assessment of Reinforced Concrete Buildings Affected by the August 10, 2025, Sındırgı (Balıkesir) Earthquake”. The authors would like to express their sincere gratitude to the Ministry of Environment, Urbanization and Climate Change (MEUCC) for providing valuable support that made this study possible. Special thanks are due to Murat Oral, Director General of Construction Affairs, Altan Özmen, Deputy Director General of Construction Affairs, and Emrah Süme, Head of the Department of Disaster Damage Assessment, for their kind assistance and contributions.

Author contributions

CRediT: Hasan Huseyin Aydogdu: Data curation, Formal analysis, Visualization, Writing - review & editing; Muhammed Sukru Yavas: Investigation, Visualization, Writing - review & editing; Ugur Demir: Investigation, Methodology, Resources, Writing - review & editing; Alper İlki: Investigation, Methodology, Resources, Supervision, Writing - review & editing.

Disclosure Statement

The authors declare that they have no known competing financial interests or personal relationships that could have appeared to influence the work reported in this paper.

Funding Declaration

Author Uğur Demir was supported by Turkish Catastrophe Insurance Pool during the post-earthquake damage process.

Data Availability Statement

The data that support the findings of this study are available on reasonable request from the corresponding author.

REFERENCES

[1] De Risi R, Sextos A, Zimmaro P, Simonelli A, Stewart J, Risi DR (2018) The 2016 Central Italy Earthquake Sequence: Observations of Incremental Building Damage. In: Proceedings of the international conference, June 2018

[2] Srinath G, Gopikrishna K (2025) Effect of repeated earthquakes on multi-storied RC buildings using IDA. Structures 79:109475. https://doi.org/10.1016/j.istruc.2025.109475

[3] Di Sarno L (2013) Effects of multiple earthquakes on inelastic structural response. Eng Struct 56:673–681, doi: 10.1016/j.engstruct.2013.05.041.

[4] Hatzivassiliou M, Hatzigeorgiou GD (2015) Seismic sequence effects on three-dimensional reinforced concrete buildings. Soil Dyn Earthq Eng 72:77–88. https://doi:10.1016/j.soildyn.2015.02.005

[5] Erdik M (2001) Report on 1999 Kocaeli and Düzce (Turkey) earthquakes. Struct Control Civ Infrastruct Eng 149-186. https://doi.org/10.1142/9789812811707_0018

[6] Saatcioglu M, Mitchell D, Tinawi R, Gardner NJ, Gillies AG, Ghobarah A, Anderson DL, Lau D (2001) The August 17, 1999, Kocaeli (Turkey) earthquake - damage to structures. Can J Civ Eng 28(4):715–737. https://doi.org/10.1139/l01-043

[7] Damci E, Temur R, Kanbir Z, Şekerci Ç, Öztorun Köroğlu E (2025) Comprehensive investigation of damage due to 2023 Kahramanmaraş earthquakes in Türkiye: causes, consequences, and mitigation. J Building Eng 99:111420. https://doi:10.1016/j.jobe.2024.111420

[8] Tapan M, Comert M, Demir C, Sayan Y, Orakcal K, Ilki A (2013) Failures of structures during the October 23, 2011 Tabanlı (Van) and November 9, 2011 Edremit (Van) earthquakes in Turkey. Eng Fail Anal 34:606–628. https://doi.org/10.101 6/j.engfailanal.2013.02.013

[9] Temur R, Damci E, Öncü Davas S, Öser C, Sarğın S, Şekerci Ç (2021) Structural and geotechnical investigations on Sivrice earthquake (Mw = 6.8), January 24, 2020. Nat Hazards 106(1):401–434. https://doi.org/10.1007/s11069-020-04468-w. Accessed 24 August 2026

[10] Yakut A, Sucuoglu H, Binici B, Canbay E, Donmez C, İlki A, Caner A, Celik OC, Ay BÖ (2022) Performance of structures in İzmir after the Samos Island Earthquake. Bull Earthq Eng 20 (14):7793–7818. https://doi:10.1007/s10518-021-01226-6

[11] Makra K, Rovithis E, Riga E, Raptakis D, Pitilakis K (2021) Amplification features and observed damages in İzmir (Turkey) due to 2020 Samos (Aegean Sea) earthquake: identifying basin effects and design requirements. Bull Earthq Eng 19(12):4773–4804. https://doi:10.1007/s10518-021-01148-3.

[12] Gurbuz T, Cengiz A, Kolemenoglu S, Demir C, Ilki A (2023) Damages and failures of structures in Izmir (turkey) during the October 30, 2020 Aegean Sea earthquake. J Eart Eng 27(6):1565–1606. https://doi:10.1080/13632469.2022.2086186

[13] Atasever K, Aydogdu HH, Narlitepe F, Goksu C, Demir U, Demir C, Ilki A (2026) Damage assessment of structures following the February 6, 2023 Kahramanmaraş earthquakes: a dataset-based case study in Gaziantep, Türkiye. Arab J Sci Eng 51(1):693–715. https://doi:10.1007/s13369-025-10991-4

[14] Vuran E, Serhatoglu C, Timuragaoglu M, Smyrou E, Bal İE, Livaoglu R (2025) Damage observations of RC buildings from 2023 Kahramanmaraş earthquake sequence and discussion on the seismic code regulations. Bull Earthq Eng 23(3):1153–1182. https://doi:10.1007/s10518-023-01843-3

[15] Pujol S, Bedirhanoglu I, Donmez C, Dowgala JD, Eryilmaz-Yildirim M, Klaboe K, Koroglu FB, Lequesne RD, Ozturk B, Pledger L, Sonmez E (2024) Quantitative evaluation of the damage to RC buildings caused by the 2023 southeast Turkey earthquake sequence. Earthq Spectra 40(1):505–530. https://doi:10.1177/87552930231211208

[16] Damci E, Temur R, Kanbir Z, Şekerci Ç, Öztorun Köroğlu E (2025) Comprehensive investigation of damage due to 2023 Kahramanmaraş earthquakes in Türkiye: causes, consequences, and mitigation. J Building Eng 99:111420. https://doi:10.1016/j.jobe.2024.111420

[17] Sezgin SK, Sakcali G, Özen S, Yıldırım E, Avcı E, Bayhan B, Çağlar N (2024) Reconnaissance report on damage caused by the February 6, 2023, Kahramanmaraş earthquakes in reinforced-concrete structures. J Build Eng 89:109200. https://doi:10.1016/j.jobe.2024.109200

[18] Aydoğdu HH, Atasever K, İlki A (2025) A pre-earthquake regional seismic risk estimation methodology and a prioritization approach for regional risk assessment. Can J Civ Eng. 53,1-19. https://doi.org/10.1139/cjce-2025-0156

[19] Maeda M, Al-Washali H (2018) Damage due to earthquakes and improvement of seismic performance of reinforced concrete buildings in Japan. In: Vacareanu R, Ionescu C (eds)

Seismic hazard and risk assessment: updated overview with emphasis on Romania. Springer, Cham, pp 361–372

[20] Di Ludovico M, Prota A, Moroni C, Manfredi G, Dolce M (2017) Reconstruction process of damaged residential buildings outside historical centres after the L'Aquila earthquake: part I: "light damage" reconstruction. Bull Earthq Eng 15(2):667–692. https://doi:10.1007/s10518-016-9877-8.

[21] Kawashima K, Aydan Ö, Aoki T, Kishimoto I, Konagai K, Matsui T, Ozkul S, Sassa K, Sassa S, Tobita Y, Toki K, Yashima A (2010) Reconnaissance investigation on the damage of the 2009 L'Aquila, Central Italy earthquake. J Earthq Eng 14(6):817–841. https://doi:10.1080/13632460903584055

[22] Kam WY, Pampanin S, Elwood K (2011) Seismic performance of reinforced concrete buildings in the 22 February Christchurch (Lyttelton) earthquake. Bull New Zeal Soc Earthq Eng 44(4):239–278

[23] Idris Y, Cummins P, Rusydy I, Muksin U, Syamsidik, Habibie MY, Meilianda E (2022) Post-earthquake damage assessment after the 6.5 mw earthquake on December, 7th 2016 in Pidie Jaya, Indonesia. J Earthq Eng 26(1):409–426

[24] Karavin YS, Akdag N, Yavas MS, Aydogdu HH, Demir U, Ilki A (2026), Seismic Reconnaissance and Structural Damage Assessment of the 10 August 2025 Sındırgı Earthquake (Mw 6.1), Türkiye "Under Evaluation of Bulletin of Earthquake Engineering Journal," 2026.

[25] Turkish Building Earthquake Code (2018) TBEC-2018. Disaster and Emergency Management Presidency, Ankara

[26] AFAD (2018) Turkish seismic hazard map. https://tdth.afad.gov.tr/TDTH/userLogin.x html. Accessed on 22 August 2026

[27] USGGS (2025) 6.0 – Sındırgı Earthquake https://earthquake.usgs.gov/earthquakes/eventpage/us6000rjsu/executive.

[28] AFAD (2025) Post-earthquake damage evaluation provisions (in Turkish). Disaster and Emergency Presidency of Türkiye. https://www.resmigazete.gov.tr/eskiler/20 25/06/20250622-1-1.pdf. Accessed 22 August 2026

[29] Ilki A, Halici OF, Comert M, Demir C (2021) The modified post-earthquake damage assessment methodology for TCIP (TCIP-DAM-2020). In: Akkar S, Ilki A, Goksu C, Erdik M (eds) Advances in assessment and modeling of earthquake loss. Springer Tracts in Civil Engineering. Springer, Cham. https://doi.org/10.1007/978-3-030-68813-4_5

[30] Jalayer F, Ebrahimian H (2017) Seismic risk assessment considering cumulative damage due to aftershocks. Earthquake Engineering & Structural Dynamics, 46(3), 369-389. https://doi:10.1002/eqe.2792

[31] Iervolino I, Chioccarelli, E, Suzuki, A (2020) Seismic damage accumulation in multiple mainshock–aftershock sequences. Earthquake Engineering & Structural Dynamics, 49(10), 1007-1027. https://doi:10.1002/eqe.3275

[32] Dedeoğlu İÖ, Yetkin M, Calayır Y (2024) Seismic performance of masonry structures in the rural area during the November 23, 2022, Düzce-Gölyaka earthquake. J Build Eng 96:110373. https://doi:10.1016/j.jobe.2024.110373

[33] Yön B (2021) Identification of failure mechanisms in existing unreinforced masonry buildings in rural areas after April 4, 2019 earthquake in Turkey. J Build Eng 43:102586. https://doi:10.1016/j.jobe.2021.102586

[34] Asteris PG, Moropoulou A, Skentou AD, Apostolopoulou M, Mohebkhah A, Cavaleri L, Rodrigues H, Varum H (2019) Stochastic vulnerability assessment of masonry structures: concepts, modeling and restoration aspects. Appl Sci 9(2):243 https://doi:10.3390/app9020243

[35] Vamvatsikos D, Pantazopoulou SJ (2016) Simplified mechanical model to estimate the seismic vulnerability of heritage unreinforced masonry buildings. J Earthq Eng 20(2):298–325. https://doi:10.1080/13632469.2015.1060583

[36] Ozdemir MA (2025) Seismic Performance Evaluation of RC–Masonry Hybrid Systems: A Comparative Study with İsa Divanli Mosque as a Case Example. Buildings 15(19):3462. https://doi.org/10.3390/buildings15193462

[37] Redmond L, Kahn L, Des Roches R (2016) Design and construction of hybrid concrete-masonry structures informed by cyclic tests. Earthq Spectra 32(4):2337–2355. https://doi:10.1193/051615EQS070M

[38] Sextos A, De Risi R, Pagliaroli A, Foti S, Passeri F, Ausilio E, Cairo R, Capatti MC, Chiabrando F, Chiaradonna A, d'Onofrio A, Dashwood B, De Silva F, de Silva F, Durante MG, Giallini V, Lanzo G, Licata V, Madiai C, Maccarini N, Marcellini A, Mylonakis G, Silvestri F, Tropeano G, Vessia G, Zimmaro P (2018) Local site effects and incremental damage of buildings during the 2016 Central Italy earthquake sequence. Earthq Spectra 34(4):1639–1669. https://doi:10.1193/100317EQS194M

[39] Graziani L, del Mese S, Tertulliani A, Arcoraci L, Maramai A, Rossi A (2019) Investigation on damage progression during the 2016–2017 seismic sequence in Central Italy using the European Macroseismic Scale (EMS-98). Bull Earthquake Eng 17(10):5535–5558. https://doi:10.1007/s10518-019-00645-w

[40] Guo X, He Z, Xu J (2020) Identification of incremental seismic damage development in RC structures excited with sequence-type ground motions. Structures 24:464–476. https://doi:10.1016/j.istruc.2020.01.012

[41] Kostinakis K, Morfidis K (2017) The impact of successive earthquakes on the seismic damage of multistorey 3D R/C buildings. Earthq Struct 12(1):1–12. https://doi:10.12989/eas.2017.12.1.001

[42] SeismoStruct (2025) A computer program for static and dynamic nonlinear analysis of framed structures. Seismosoft. http://www.seismosoft.com

[43] Mander JB, Priestley MJ, Park R (1988) Theoretical stress-strain model for confined concrete. J Struct Eng 114(8):1804–1826. https://doi.org/10.1061/(ASCE)0733-9445(1988)114:8(1804)

[44] Menegotto M, Pinto PE (1973) Method of analysis for cyclically loaded R.C. plane frame including changes in geometry and non-elastic behaviour of elements under combined normal force and bending. In: Proceedings of IABSE symposium on resistance and ultimate deformability of structures acted on by well defined repeated loads, Lisbon, vol 11, pp 15–22.

[45] FEMA (1998) Evaluation of earthquake damaged concrete and masonry wall buildings. Report No. FEMA 306, Federal Emergency Management Agency, Washington, D.C.

[46] Halici Ö, Demir U, Zabbar Y, Ilki A (2023) Out-of-plane seismic performance of bed-joint reinforced autoclaved aerated concrete (AAC) infill walls damaged under cyclic in-plane displacement reversals. Eng Struct 286:116077. https://doi.org/10.1016/j.engstruct.2023.116077

[47] Ilki A, and Celep Z (2012) Earthquakes, existing buildings and seismic design codes in Turkey. Arabian Journal for Science and Engineering 37(2):365-380. https://doi.org/10.1007/s13369-012-0183-8